Available online at www.sciencedirect.com

ScienceDirect

Geochimica et Cosmochimica Acta 288 (2020) 138–160

Geochimica et Cosmochimica Acta

www.elsevier.com/locate/gca

A comparison of marine Fe and Mn cycling: U.S. GEOTRACES GN01 Western Arctic case study

Laramie T. Jensen [a], Peter Morton [b], Benjamin S. Twining [c], Maija I. Heller [d,e,f], Mariko Hatta [g], Christopher I. Measures [g], Seth John [h], Ruifeng Zhang [h,i], Paulina Pinedo-Gonzalez [h,j], Robert M. Sherrell [k], Jessica N. Fitzsimmons [a,*]

[a] *Department of Oceanography, Texas A&M University, College Station, TX 77840, USA*
[b] *National High Magnetic Field Laboratory, Florida State University, 1800 E. Paul Dirac Drive, Tallahassee, FL 32310, USA*
[c] *Bigelow Laboratory for Ocean Sciences, 60 Bigelow Drive, East Boothbay, ME 04544, USA*
[d] *Department of Ocean Sciences, University of California, Santa Cruz, CA 95064, USA*
[e] *Escuela de Ciencias del Mar, Facultad de Ciencias del Mar y Geografia , Pontifica Universidad Católica de Valparaiso, Valparaiso, Chile*
[f] *Instituto Milenio de Oceanografia, Casilla 1313, Concepcion, Chile*
[g] *Department of Oceanography, University of Hawaii at Manoa, 1000 Pope Road, Honolulu, HI 96822, USA*
[h] *Department of Earth Sciences, University of Southern California, Los Angeles, CA, USA*
[i] *School of Oceanography, Shanghai Jiao Tong University, Shanghai 200030, China*
[j] *Lamont-Doherty Earth Observatory of Columbia University, Post Office Box 1000, Palisades, NY 10964, USA*
[k] *Department of Marine and Coastal Sciences and Department of Earth and Planetary Sciences, Rutgers University, 71 Dudley Road, New Brunswick, NJ 08901, USA*

Received 20 April 2020; accepted in revised form 8 August 2020; available online 17 August 2020

Abstract

Dissolved iron (Fe) and manganese (Mn) share common sources and sinks in the global ocean. However, Fe and Mn also have different redox reactivity and speciation that can cause their distributions to become decoupled. The Arctic Ocean provides a unique opportunity to compare Fe and Mn distributions because the wide Arctic continental shelves provide significant margin fluxes of both elements, yet *in situ* vertical regeneration inputs that can complicate scavenging calculations are negligible under the ice of the Arctic Ocean, making it easier to interpret the fate of lateral gradients. We present here a large-scale case study demonstrating a three-step mechanism for Fe and Mn decoupling in the upper 400 m of the Western Arctic Ocean. Both Fe and Mn are released during diagenesis in porewaters of the Chukchi Shelf, but they become immediately decoupled when Fe is much more rapidly oxidized and re-precipitated than Mn in the oxic Chukchi Shelf water column, leading to Fe hosted primarily in the particulate phase and Mn in the dissolved phase. However, as these shelf fluxes are transported toward the shelf break and subducted into the subsurface halocline water mass, the loss rates of all species change significantly, causing further Fe and Mn decoupling. In the second decoupling step in the shelf break region, the dominant shelf species are removed rapidly via particle scavenging, with smallest soluble Fe (sFe < 0.02 μm) being least subject to loss, while colloidal Fe (0.02 μm $<$ cFe < 0.2 μm), dissolved Mn (dMn), and non-lithogenic particulate Fe (pFe_{xs}) are all lost at similarly rapid rates. In the third decoupling step, once these species are swept >1000 km offshore with the prevailing current into the low-particle waters of the open Arctic, cFe and dMn appear conserved, while pFe, dFe, and sFe are very slowly removed with variable log-scale distances of transport: pFe $\ll$ dFe $<$ sFe. To assess the role of physicochemical speciation on these trends, we observed that Fe(II) was a small (~7%) fraction of total dFe in the upper 400 m of the Arctic, even over the shelf (~2%). Also, colloidal contribution to dFe was very low (~20%) in the open Arctic, in contrast to dFe in the North

* Corresponding author.
E-mail address: jessfitz@tamu.edu (J.N. Fitzsimmons).

https://doi.org/10.1016/j.gca.2020.08.006

Atlantic, which is composed much more by colloids (≥50%). Throughout the Western Arctic Ocean, Fe and Mn are thus decoupled as a result of distinct oxidation kinetics and different scavenging rates within high- and low-particle regimes. As the "scavengers of the sea", the relative distribution of particulate Fe and Mn phases across the Arctic Ocean shelf and slope, respectively, will play an important role in determining the distribution and ultimate sediment burial site for other scavenging-prone trace elements. Additionally, we suggest that the future effects of climate change, including loss of sea ice that could impact the formation of the halocline, might change distributions of Fe and Mn species in the future Western Arctic.

Keywords: Iron; Manganese; Colloids; Diagenesis; Sediments; Halocline; Arctic Ocean; GEOTRACES

1. INTRODUCTION

Iron (Fe) and manganese (Mn) are both essential micronutrients for marine phytoplankton as well as important tracers of redox processes in the global ocean. These metals share common sources (Fig. 1), including diagenetic release from sediments (Froelich et al., 1979), hydrothermal vent fluxes (German et al., 2016), and dust inputs (Arimoto et al., 1985; Boyle et al., 2005; Shiller, 1997). They are also subject to similar removal processes such as biological uptake (Sunda, 2012; Sunda and Huntsman, 1995, 1998), oxidative precipitation (Bruland and Lohan, 2003), flocculation in estuaries (Sholkovitz et al., 1978; Sholkovitz, 1978), and scavenging (Balistrieri et al., 1981; Martin and Knauer, 1985). Both Fe and Mn have a significant particulate fraction due to a combination of their high concentrations in lithogenic particles, their propensity towards oxidative precipitation, and their abundance within cells in the surface ocean, leading to subsurface remineralization back to the dissolved phase during the decay of organic matter. These commonalities often lead to studies comparing dissolved Fe and Mn fluxes and distributions, particularly in hydrothermal and margin environments, where their coupled enrichments can be used as indicators of a common source flux (Boyle et al., 2005; Bucciarelli et al., 2001; Chase et al., 2005; Colombo et al., 2020; Cowen and Bruland, 1985; Fitzsimmons et al., 2014, 2017; Hatta et al., 2015; Lam and Bishop, 2008; Landing and Bruland, 1987; Lewis and Landing, 1991; Noble et al., 2012; Saager et al., 1989; Sanial et al., 2017; Sedwick et al., 2000, 1997; Sherrell et al., 2018). Seminal studies comparing the marine geochemical behavior of these two elements, such as Landing and Bruland (1987), have set the stage for examining Fe and Mn cycling and transformations across a suite of complex environments.

However, despite similarities in their distributions resulting from their shared source fluxes, Fe and Mn have quite disparate speciation and reactivity that cause them

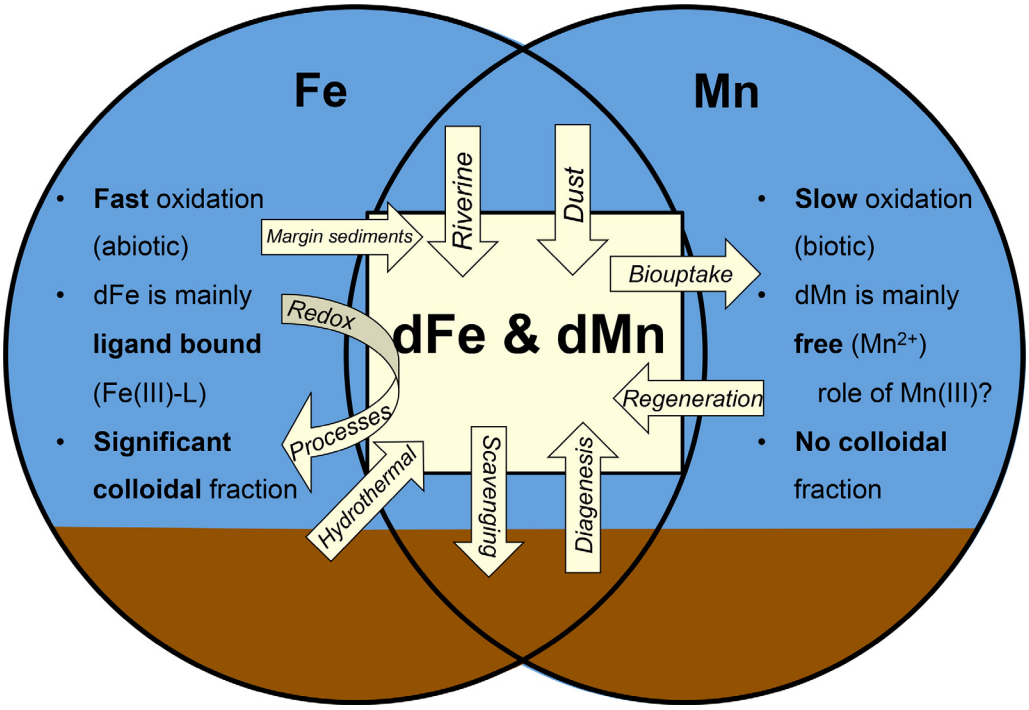

Fig. 1. Schematic of the similarities and differences between Fe and Mn highlighted in this study. The two elements share similar sources and sinks but differing chemistries. Blue represents water and brown represents the sediments.

to become decoupled in the ocean (Fig. 1). The best example of this is their oxidation kinetics. While both Fe(II) and Mn(II) are produced during sediment diagenesis (Froelich et al., 1979), Fe(II) oxidizes rapidly and abiotically to Fe (III) oxides in the presence of oxygen, often within minutes in fully oxygenated seawater (Millero et al., 1987), while Mn(II) oxidizes more slowly to Mn(III)/Mn(IV), and this process often requires microbial mediation (Stumm and Morgan, 1981; Tebo et al., 2004; Yu and Leadbetter, 2020). These differences in oxidation rate decouple the dissolved Fe and Mn distributions in surface waters, where photochemical reduction of MnO_2(s) to Mn^{2+} allows dissolved Mn to be retained in the surface ocean (Sunda et al., 1983; Sunda and Huntsman, 1994); in contrast, any photochemical reduction of analogous solid Fe(III) oxyhydroxides would be quickly reversed by reoxidation, preventing surface accumulation of dFe species (Barbeau et al., 2001). Additionally, while both Fe(III) and Mn(IV) are insoluble under seawater conditions (Kuma et al., 1996; Liu and Millero, 2002; Sunda et al., 1983), only Fe is appreciably stabilized by organic ligands in the water column (Bruland and Lohan, 2003; Gledhill and Buck, 2012). While Mn(III) bound to organic ligands has been found to have a variable contribution to total dissolved Mn in coastal areas, continental margin, and hydrothermal sites (Chen et al., 2019; Madison et al., 2013; Oldham et al., 2017, 2015), most dissolved Mn in the open ocean is thought to exist in the free Mn^{2+} form (Byrne, 2002). Together, these differences in oxidation pathways and speciation can lead to different trajectories and residence times of Fe and Mn in the ocean, including shorter dFe residence times in the upper water column, and longer dFe residence times in the deep water (Bruland et al., 1994; Landing and Bruland, 1987).

Some prior studies have compared the distributions and cycling of Fe and Mn (Chase et al., 2005; Cheize et al., 2019; Colombo et al., 2020; Fitzsimmons et al., 2017; Hatta et al., 2015; Landing and Bruland, 1987; Lewis and Landing, 1991; Noble et al., 2012, 2008). However, the Arctic Ocean is unique compared to these previously studied sites because it is dominated by shallow continental shelves (>50% by area (Jakobsson et al., 2004; Talley et al., 2011)) and is largely isolated because of limited exchange with the Atlantic and Pacific Oceans (Talley et al., 2011). The waters of the Arctic's highly productive Chukchi Shelf, which receives nutrient-rich inputs through the Bering Strait (Anderson et al., 2013; Jones and Anderson, 1986), are carried offshore into the open Western Arctic within the halocline, a high-salinity water mass that forms during sea ice formation from brine rejection of Arctic shelf waters. Arctic shelf waters are in contact with shelf sediments over the shallow Chukchi Shelf, such that the Western Arctic halocline uniquely carries a large sedimentary flux of redox-active metals far into the Canada Basin of the Western Arctic (Aguilar-Islas et al., 2013; Cid et al., 2012; Kondo et al., 2016; Nakayama et al., 2011; Nishimura et al., 2012). The Western Arctic's halocline is also special because, although some algae do grow directly under the sea ice in this region (Arrigo et al., 2012; Sakshaug, 2004), *in situ* vertical remineralization fluxes through the halocline are very limited for metal micronutrients and macronutrients, especially farther away from the shelves where few sinking cells grow under the ice (Jensen et al., 2019; Klunder et al., 2012a, 2012b; Kondo et al., 2016; Middag et al., 2011). Thus, the Western Arctic's shelf signal remains relatively undisturbed by vertical remineralization inputs from biogenic particles sinking into the central Arctic and can be used to trace the effects of aging shelf fluxes to the open ocean with little correction for other processes.

For these reasons, the Arctic Ocean provides an ideal location in which to examine the contrasting chemistry of Fe and Mn. Here, we present Fe and Mn data from the U.S. Arctic GEOTRACES GN01 transect to examine the effects of long-range transport of Fe and Mn from shelf sources as well as surface oxidation rates. The large spatial scale of our GN01 Western Arctic study provides a critical link between high productivity shelf regimes with open ocean circulation in a rapidly changing environment, both seasonally and inter-annually with ongoing climate change (Harrison and Cota, 1991; Hill and Cota, 2005; Lepore et al., 2007). Our results show that Fe and Mn have decoupled cycles in the Western Arctic with a distinct three-step pattern of differentiation. We find (1) rapid Fe oxidation to the particulate phase over the Chukchi Shelf compared to Mn due to a difference in oxidation kinetics, (2) rapid removal of both dFe and dMn resulting from interaction with the high particle concentrations over the outer shelf and shelf break, followed by (3) slower scavenging of dFe away from the shelf while dMn remains conserved. This is in line with a common diagenetic source of Fe and Mn that is not equally preserved due to differences in oxidation kinetics and proclivity to scavenging. While these processes have been identified previously, the Western Arctic provides an excellent opportunity to assess the differences in the geochemical cycling of these two important metals.

2. SAMPLE COLLECTION AND ANALYSIS METHODS

Seawater samples for this study were collected during the 2015 U.S. Arctic GEOTRACES cruise (GN01), which departed from Dutch Harbor, AK aboard the USCGC *Healy* (HLY1502) and continued from 9 August 2015 to 12 October 2015. The cruise track (Fig. 2) originated in the North Pacific in the Bering Sea and transited north, entering the Arctic Ocean through the Bering Strait and continuing to the North Pole ("northbound") along ~170–180°W before returning along 150°W ("southbound") and terminating on the Chukchi Shelf. Samples were taken in the Canada, Makarov, and Amundsen basins in the Western Arctic, along the shelf, within the marginal ice zone, and at shallow-depth ice hole stations. While many stations were full-depth (0–4000 m), only data from the upper 400 m are reported in this study.

Dissolved and particulate trace metal sample collection followed established GEOTRACES protocols (Cutter et al., 2010). Seawater was first collected using a trace metal-clean carousel/CTD (Sea-Bird) with a conductive Vectran-coated cable and 24 × 12 L Go-Flo bottles (General Oceanics). Two Go-Flo bottles were tripped per sampling depth on ascent at ~3 m/min and were pressurized

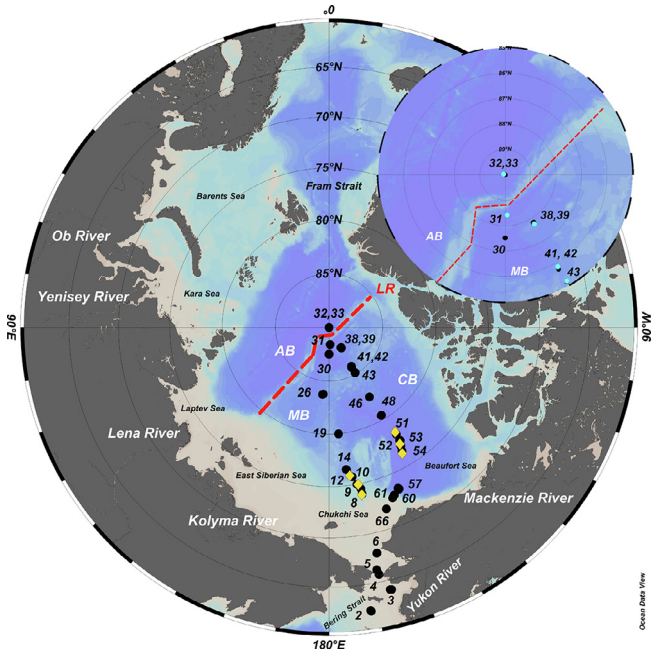

Fig. 2. U.S. GEOTRACES Arctic GN01 transect with relevant stations, rivers, seas, and bathymetric features identified. Blue dots in inset = ice Stations 31, 33, 39, 42, 43, gold diamonds = MIZ Stations 8, 9, 10, 12, 52, 53, 54, black dots = full depth stations. AB = Amundsen Basin, MB = Makarov Basin, CB = Canada Basin, LR = Lomonosov Ridge. Stations 2–5 are considered "Bering Strait" while stations 6–8 and 66–61 are "Chukchi Shelf." Stations 8–31 are "northbound" transect, Station 32 is the North Pole, and Stations 38–66 are "southbound" transect. More detail can be found in Jensen et al. (2019).

(~0.5 atm) with HEPA-filtered air during sub-sampling. One of the two Go-Flo bottles was fitted with a 0.2 µm AcroPak-200 polyethersulfone filter capsule (Pall), and seawater was subsequently filtered into 250 mL acid pre-cleaned low density polyethylene (LDPE) Nalgene bottles following three 10% volume sample rinses of the bottle, cap, and threads (Fitzsimmons and Boyle, 2012). Samples were promptly acidified to pH < 2 (0.012 M HCl, Optima, Fisher Scientific).

The second Go-Flo bottle was used to collect particle samples, following the techniques of Planquette and Sherrell (2012). Immediately before sampling, each Go-Flo was gently inverted to homogenize the particle distribution and then fitted with a 0.45 µm polyethersulfone Supor filter in a polypropylene Swinnex filter holder. Process blanks were generated by passing filtered seawater (<0.2 µm AcroPak filtered) through the same Supor-substrate filters used for samples.

Surface and near-surface ice hole samples (Stations 31, 33, 39, 43) were collected by small boat or through holes in the sea ice at 1, 5, and 20 m using a polypropylene high-head battery-powered motor diaphragm pump (Cole Parmer) with ½-inch FEP-lined Tygon tubing fitted with a pre-cleaned 0.2 µm AcroPak filter. Samples were filtered on the ice into a 25 L acid-cleaned LDPE carboy and immediately subsampled into clean LDPE bottles on the ship.

2.1. Ultrafiltration

Following collection, filtered (0.2 µm) seawater was immediately brought into a shipboard clean lab (plastic "bubble" under positive pressure via HEPA-filtered air) for further ultrafiltration into soluble size fractions. Ultrafiltration using Anopore filters was carried out at all stations and depths where dissolved samples were collected, and ultrafiltration was completed within 3 hours of collection to prevent bottle effects (Jensen et al., 2020). This direct ultrafiltration system employed custom-made filtration rigs and vacuum filtration (<0.5 atm) and used 0.02 µm Anodisc filters (47 mm Anopore membranes, Whatman) that were cleaned on the rig with ~50 mL dilute HCl (~0.005 M, pH < 2, Optima) followed by ~50 mL ultrapure MQ water, and finally conditioned with ~50 mL of the seawater sample, all immediately before filtering the sample (Fitzsimmons and Boyle, 2014a). Seawater (<0.2 µm) was poured onto the filtration rig under vacuum (<0.5 atm) until each LDPE (Nalgene) 60 mL bottle was filled, following a 10% rinse of the bottle, cap, and threads. All samples were promptly acidified to 0.012 M HCl (Optima, Fisher Scientific) (Fitzsimmons and Boyle, 2012). Colloidal concentrations (cFe) were calculated by subtracting the soluble Fe concentration (sFe, permeate) from the dissolved concentration, i.e. $cFe = dFe - sFe$.

2.2. Dissolved analyses

Acidified samples were kept for at least nine months following acidification, allowing adequate time for complete desorption of metals from bottle walls (Jensen et al., 2020). Following this period, samples were pre-concentrated for dissolved Fe and Mn using a SeaFAST-pico system (ESI, Omaha, NE) at Texas A&M University

using an isotope dilution and standard curve method modified from Lagerström et al. (2013) and described previously (Jensen et al., 2020). Other elements concurrently analyzed were Zn and Cd (Jensen et al., 2019; Zhang et al., 2019), and Ni, Cu, and Pb, which will be published separately. For each sample, a 10 mL aliquot of seawater was weighed and spiked with a known isotopic composition of ^{57}Fe and loaded into the SeaFAST system. Manganese is a monoisotopic element, and so instead of isotope dilution, Mn was quantified using a six-point Mn standard curve spanning additions of 0–10 nmol/kg (and further up to 80 nmol/kg for shelf stations) made in matrix-matched, low-metal seawater and also processed through the SeaFAST system. Once loaded onto the SeaFAST, all samples were buffered in-line to pH ~ 6.3 with an ammonium acetate buffer (Optima, Fisher Scientific) and loaded onto a column fitted with Nobias-chelate PA1 resin and rinsed with buffered ultrapure water to remove any salts. Following metal extraction onto the resin, samples were back-eluted with 10% (v/v) nitric acid ($HN0_3$, Optima) into 400 µL of eluent (25× pre-concentration factor) for analysis. Pre-concentrated eluents were subsequently analyzed in medium resolution for Fe and Mn on a Thermo Element XR high-resolution inductively-coupled plasma mass spectrometer (HR-ICP-MS) housed at the R. Ken Williams Radiogenic laboratory at Texas A&M University. Accuracy, precision and limits of detection of these measurements are summarized in Table 1.

2.3. Particulate analyses

All filters for particle analyses were stored frozen until they were digested in acid-cleaned perfluoroalkoxy alkane (PFA) vials (Savillex) by adding 2 mL of a mixture of 4 M HCl, 4 M HNO_3, and 4 M hydrofluoric acid (Optima, Fisher Scientific) and heated at 110 °C for four hours (Ohnemus and Lam, 2015; Twining et al., 2015). The digest solution was carefully poured into a second Savillex vial without transferring the Supor filter itself, and 60 µL of concentrated H_2SO_4 (18.4 M; Fisher Optima grade) and 20 µL of H_2O_2 (9.8 M; Fisher Optima grade) were added to the solution to break down any Supor filter fragments. The solution was taken to dryness and the residue re-dissolved with 0.32 M HNO_3 (Fisher Optima or double-distilled grade) containing 10 ppb In to correct for matrix effects and instrumental drift. The analytical assessments including blanks and reference material recoveries are shown in Table 1. All particulate values reported here are the non-lithogenic or "excess" fraction (shown here as p$[Metal]_{xs}$), determined by applying the metal/Al crustal abundance ratio from Rudnick and Gao (2003) and then multiplying by the pAl concentration, assuming all pAl is

Table 1
Reported certified SAFe D1, D2, and S values as well as blanks and detection limits for dissolved Fe and Mn. Reported certified and consensus values as well as blanks and detection limits for Total particulate Fe and Mn.

Sample		Element (nmol/kg)		Sample		Element (µg/g)	
	n	dFe	dMn		n	Total pFe	Total pMn
SAFe D1	35	0.602	0.395	**BCR-414**	5	**1737**	**253**
1SD		0.059	0.02	**1SD**		**41**	**10**
Consensus (May 2013)*		0.67	0.35	Certified		1850**	299
1SD		0.04	0.05	1SD		190	12
SAFe S	4	0.085	0.869	**NRC MESS-3**	5	**41,800**	**322**
1SD		0.038	0.011	**1SD**		**1700**	**16**
Consensus (May 2013)		0.093	0.79	Certified		43,400	324
1SD		0.008	0.06	1SD		1100	12
GSP	12	0.159	0.757	**NRC PACS-2**	4	**41,300**	**1070**
1SD		0.03	0.025	**1SD**		**300**	**44**
Consensus (2019)		0.155	0.778	Certified		40,900	960
1SD		0.045	0.034	1SD		600	40
GSC	12	1.65	2.109				
1SD		0.062	0.11				
Consensus (2019)		1.535	2.18				
1SD		0.115	0.075				

		Element (nmol/kg)			Element (nmol/kg)	
	n	Fe	Mn	n	Total Fe	Total Mn
Average blank	31	0.0635	0.0005	21	0.044	0.0033
Detection limit (3 × 1SD of blank)	29	0.0174	0.0001	21	0.094	0.0073

* Value for dMn from SAFe D2 consensus (May 2013).
** Informational, non-certified value reported by CRM distributor.

lithogenic, and subtracting this lithogenic term from the overall particulate metal concentration. This lithogenic correction was an average of 7 ± 3% and 7 ± 13% of the total labile particulate phase for Fe and Mn, respectively, across the shelf and offshore waters.

2.4. Intercalibration of dissolved Fe and Mn datasets

The U.S. GEOTRACES GN01 effort to measure dissolved metals encompassed multiple laboratories, methods, and analyses. Dissolved Fe and Mn analyses took place at Texas A&M University, the University of Southern California, and shipboard by the team from the University of Hawaii (methods used by these laboratories are described in the Supplementary Information). The three dissolved metal datasets agreed well at the subset of stations where they were intercalibrated (Fig. S1), and the Texas A&M University dataset is reported in this manuscript, for convenience.

2.5. Hydrographic analyses

Salinity, macronutrients and other hydrographic variables were determined shipboard by the Scripps Institute of Oceanography Ocean Data Facility (SIO ODF) team. Temperature and pressure for all samples were taken directly from the trace metal CTD (Sea-Bird 911+) sensors. Bottle salinity, collected from the same Go-Flos used for metal analyses, was measured unfiltered at room temperature on a shipboard Guideline Autosal 8400B salinometer. Dissolved macronutrients nitrate, phosphate, and silicate collected from the same Go-Flo bottles as the metals were analyzed shipboard at room temperature on a Seal Analytical continuous-flow AutoAnalyzer 3 (Hydes et al., 2010). Depth-matched dissolved oxygen samples were collected using a 36-place, ~10 liter Niskin bottle rosette equipped with a Sea-Bird SBE9 + CTD and other sensors operated by the SIO ODF team and analyzed shipboard using a Winkler titration method (Carpenter, 1965; Culberson et al., 1991). Data can be found at: https://www.bco-dmo.org/dataset/647259. All surface and contoured sections in this paper were made using Ocean Data View software (Schlitzer, 2016).

3. RESULTS AND DISCUSSION

3.1. Hydrography

The hydrography of the upper 400 m of the Western Arctic is defined by water masses with unique thermohaline and macronutrient structure (Aagaard et al., 1985; Rudels, 2015). Briefly, along the GN01 section, four major water masses were observed (Jensen et al., 2019): (1) the surface polar mixed layer (sPML) extending 0–25 m (salinity, S of 25–31), (2) the upper halocline layer (UHL), extending ~50–150 m (S of 31–33.1), (3) the lower halocline layer (LHL) waters extending ~150–400 m (S of 33.1–34.7), and (4) the Makarov/Amundsen basins' single halocline, extending from ~50–300 m (S of 31–34.3). Importantly, the UHL and LHL were observed only in the Canada Basin (GN01 Stations 10–19, 46–60). The UHL results from nutrient-rich Pacific waters entering through the shallow Bering Strait and becoming entrained via brine rejection into this subsurface water mass (Shimada et al., 2005; Woodgate et al., 2005); as such, we define the UHL as having [Si] > 25 μmol/kg (Anderson et al., 2013; Jones and Anderson, 1986; Macdonald et al., 1989) and centering on S of 32.8 (Fig. 3a, b). In contrast, the LHL originates in the Eastern Arctic on the Eurasian shelves and can be traced using a minimum in the conservative tracer NO ($NO = [O_2] + 9[NO_3^-]$), following the work of Jones and Anderson (1986) (Fig. 3a). Along GN01, the LHL has depths 150–400 m under the UHL near the shelf and shoals to depths of 100–200 m further offshore. Similarly, the single halocline was found only in the Makarov and Amundsen basins (Stations 26–43), and was also formed on Eurasian shelves and advected into both the Amundsen and then the Makarov across the Lomonosov Ridge (Rudels, 2015).

3.2. Overview of Fe and Mn Observations

Dissolved and excess particulate Fe and Mn concentrations (shown as dFe, pFe_{xs}, dMn, pMn_{xs}) varied by orders of magnitude in the upper 400 m of the Western Arctic (Fig. 3), demonstrating the inherent diversity in source and evolution of these redox-sensitive metals. Nonetheless, the concentrations reported here compare well with previous reports of the geochemistry of the Canada Basin (Aguilar-Islas et al., 2013; Cid et al., 2012; Kondo et al., 2016), as well as in the Makarov and Amundsen basins (Klunder et al., 2012a; Middag et al., 2011).

The widest concentration range was found along the dynamic Chukchi Shelf and Bering Strait (Stations 2–8, 61–66, depth 0–80 m), where dFe ranged from 0.24 to 19.6 nmol/kg, dMn from 3.81 to 197 nmol/kg, non-lithogenic pFe_{xs} from 0 to 2130 nmol/kg, and pMn_{xs} from 0 to 17.4 nmol/kg. Within surface waters (Fig. 4), dFe decreased rapidly from a broad average of 3.19 ± 2.65 nmol/kg over the shelf/strait stations to 0.521 ± 0.100 nmol/kg off shelf (Stations 10–12, 57–60), with an increase again at the North Pole due to the Transpolar Drift current that supplies riverine Fe from the Eurasian continent, which is the subject of another paper (Charette et al., 2020). In contrast, elevated dMn extended further off-shelf, decreasing progressively from 23.6 ± 10.8 nmol/kg over the shelf/strait to 2.61 nmol/kg at the North Pole. In the particulate fraction, surface pFe_{xs} was high over the shelf (as high as 346 nmol/kg at Station 5) and decreased dramatically off-shelf, to a minimum of 0.33 nmol/kg (Station 31), while surface pMn_{xs} was quite low and inconsistently distributed, roughly decreasing from 10.0 nmol/kg along the shelf to negligible concentrations in the central Arctic (Fig. 4c, d). Thus, overall surface Fe was dominated by particles, while surface Mn was dominated by dissolved species (Fig. 4b).

Within the Canada Basin UHL ([Si] > 25 μmol/kg, Stations 8–19, 46–60), dFe and dMn showed local maxima (Fig. 3). In the UHL, dFe ranged from 0.45 nmol/kg to 3.82 nmol/kg (average 0.96 ± 0.73 nmol/kg), and the contribution of dFe to the "total labile" Fe pool (dFe + pFe_{xs})

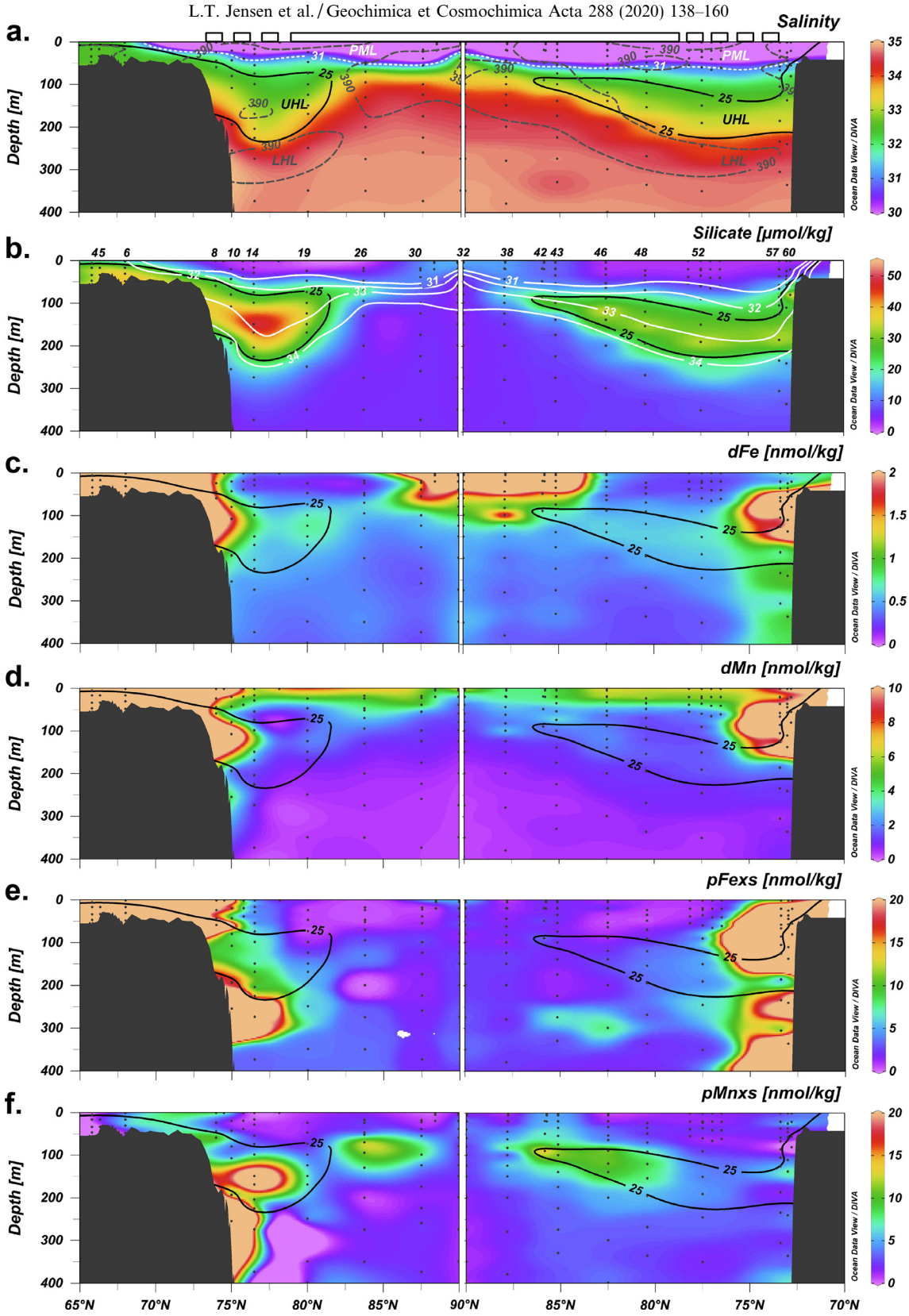

Fig. 3. Sectional plots of (a) salinity, (b) silicate, (c) dFe, (d) dMn, (e) pFe_{xs} (particulate Fe excess), (f) pMn_{xs} (particulate Mn excess) in the upper 400 m. Silicate contour line for [Si] = 25 µmol/kg is overlaid in black to denote the bounds of the Upper Halocline layer (UHL; see text) for all plots. In plot a) the Polar Mixed layer (PML) is labeled and denoted by a white salinity contour line (S = 31; see text) and the Lower Halocline layer (LHL) is labeled and denoted by a gray NO contour line (NO = 395 µmol/kg; see text). In plot b) the white contour lines represent salinity. Transect progressed northbound from Station 4 to Station 30 (left panels) and then southbound from the North Pole (Station 32) to the shelf break (Station 60, right panels). Regions of sea ice coverage are indicated by a white bar at the top of the figure, and the Marginal Ice Zone (MIZ) is indicated by a broken white bar.

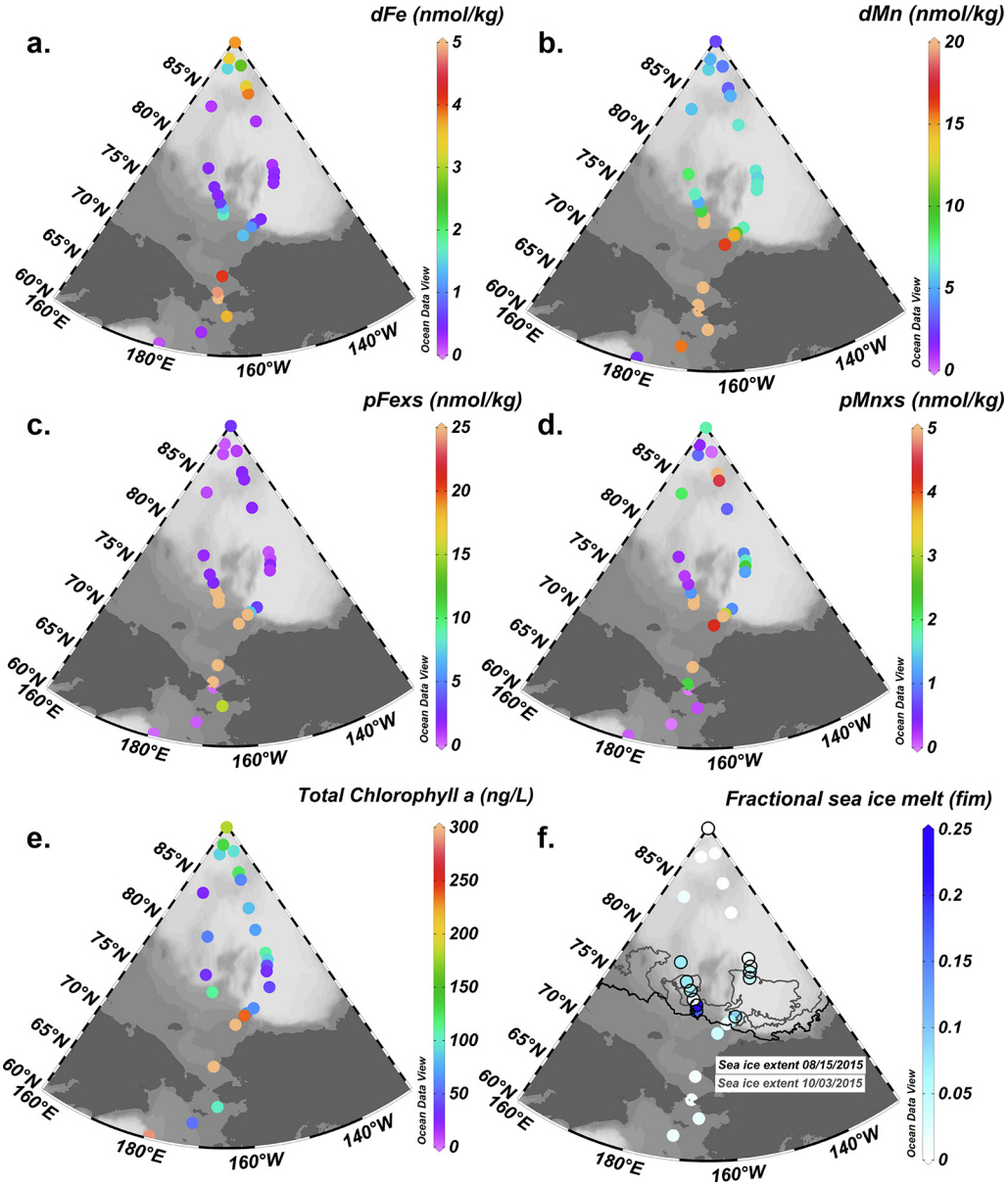

Fig. 4. Surface (0–20 m) plots of (a) dFe, (b) dMn, (c) pFexs, (d) pMnxs, (e) total chlorophyll a and (f) fractional ice melt (fim). Plot (f) shows sea ice extent on August 15th, 2015 when Station 8 was sampled (black) and on October 3rd, 2015 when Station 57 was sampled (grey) to show the extent of the Marginal Ice Zone (MIZ; stations symbols outlined in black in plot f).

changed with distance from the shelf break (Fig. 5). The dFe fraction (dFe/(dFe + pFe_{xs})) composed <20% of total labile Fe at stations within 900 km of the shelf break (Stations 8, 10, 14, 48, 52, 57, 60) and increased to 15–63% of total labile Fe at distances greater than 900 km (Stations 19, 46). Likewise, dMn ranged from 1.19 to 25.1 nmol/kg (average 4.38 ± 5.98 nmol/kg) comprising 20–85% of total labile Mn (Fig. 5b) within 900 km of the shelf break and a smaller 20–50% at distances greater than 900 km. Excess particulate Fe ranged from 0.311 to 142 nmol/kg (average 15.77 ± 31.60 nmol/kg) and pMnxs from 1.71 to 37.0 nmol/kg (average 8.51 ± 8.56 nmol/kg). The dissolved values agreed well with previous studies of the Canada Basin UHL (Aguilar-Islas et al., 2013; Kondo et al., 2016; Colombo et al., 2020).

In the deeper Canada Basin LHL (150–400 m), concentrations for all species were, on average, lower than in the UHL. Dissolved Fe averaged 0.611 ± 0.246 nmol/kg, dMn at 1.10 ± 0.39 nmol/kg, pFe_{xs} at 10.0 ± 10.6 nmol/kg, and pMn_{xs} at 4.88 ± 2.35 nmol/kg. Within the Eurasian shelf-influenced Makarov/Amundsen halocline (Stations 26, 30, 32, 38, 43), we eliminated any depths with clear transpolar drift (TPD) influence; this surface current dominated dFe and dMn patterns in the upper 80 m of the water column (Charette et al. 2020). For reference, at the TPD influenced depths, dFe averaged 0.54 ± 0.09 nmol/kg,

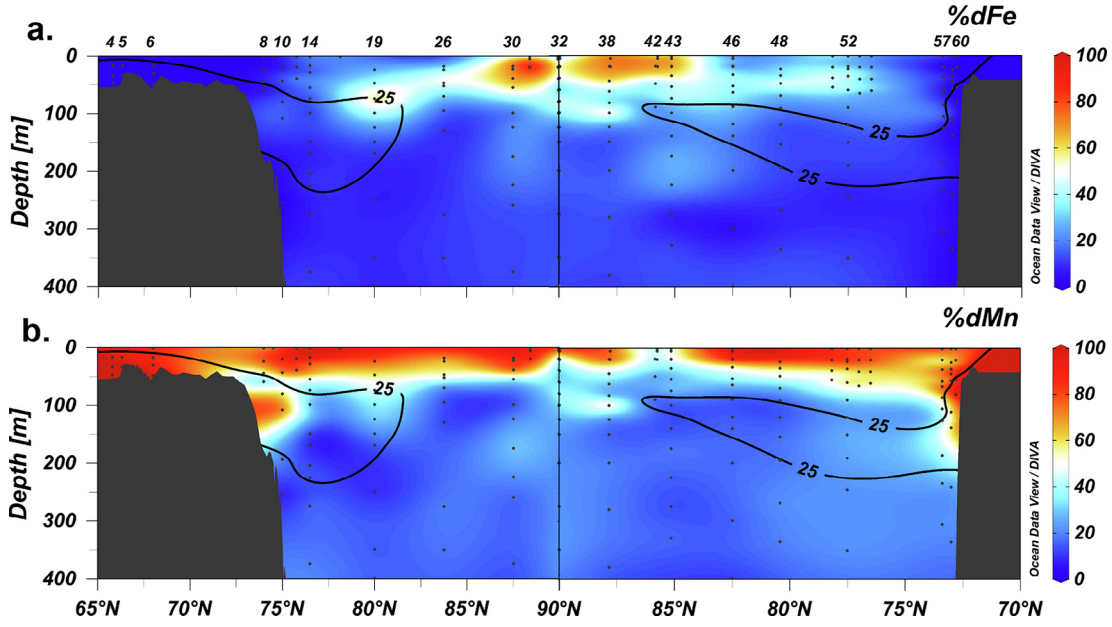

Fig. 5. Plots of (a) %dFe = dFe/(dFe + pFe_{xs}) and (b) %dMn = dMn/(dMn + pMn_{xs}) across the upper 400 m of the transect moving northbound (left panel) to the North Pole and then southbound (right panel). All percentage values range 0–100% to show the influence of the dissolved phase on the total labile (dissolved and particulate) metal content. Silicate contours in black ([Si] = 25 μmol/kg) denote the bounds of the UHL.

dMn 1.71 ± 0.85 nmol/kg, pFe_{xs} 2.43 ± 1.01 nmol/kg, and pMn_{xs} 8.97 ± 4.61 nmol/kg.

3.2.1. Marginal Ice Zone (MIZ)

Sea ice can be an important source of dissolved and particulate Fe and Mn in the Arctic and other polar regions. Previous studies have shown elevated dFe in sediment-laden Arctic sea ice (up to ~3600 nmol/kg, (Tovar-Sánchez et al., 2010)) and point to sea ice melting as a potentially significant dFe and pFe source (Aguilar-Islas et al., 2008; Kanna et al., 2014; Measures, 1999; Tovar-Sánchez et al., 2010). During GN01, reported dFe concentrations in sea ice (1.1 ± 1.0 nmol/kg (Marsay et al., 2018)) were very low, likely due to brine drainage of first-year ice so late in the summer season (Nakawo and Sinha, 1981; Vancoppenolle et al., 2006). In contrast to Fe, little is known about Mn in Arctic sea ice, though both dMn and pMn are known to be quite low in Antarctic sea ice (less than 1.5 and 5 nmol/kg, respectively (Lannuzel et al., 2011)). Dissolved Mn was more elevated in sea ice from the central Arctic during GN01 (6.0 ± 4.2 nmol/kg (Marsay et al., 2018)), despite the brine drainage.

During GN01, sea ice met open ocean water near the Chukchi Shelf break at what is termed the Marginal Ice Zone (MIZ). The fraction of each water sample that derives from melted sea ice was mapped in the MIZ using oxygen isotopes in seawater (Newton et al., 2013), here referred to as fractional ice melt ("fim"). Fractional ice melt was highest across stations 8–17 (northbound) and 51–57 (southbound), showing a 1.5 – 23% contribution from sea ice melt to total water budgets at these stations (Fig. 3a and Fig. 4). At all ice-influenced stations, we assessed the relationship between dFe, dMn, pFe_{xs}, and pMn_{xs} with fim in the upper 1–10 m (Fig. 6) to determine whether ice was a source or diluent of each metal. This relationship also allowed us to assess whether surface metals reflected conservative mixing between surface seawater and ice melt (producing a straight line) or whether there was non-conservative metal addition from sea ice sediments or removal via biological uptake in the MIZ (curved lines). One caveat is that shallow Shelf Stations 8–10 (shown as open circles in Fig. 6) were likely influenced by shelf inputs of dFe, dMn, and pFe_{xs}, and thus the metal concentrations may not be attributable solely to sea ice fluxes; thus, we have removed those stations from our sea ice melt analysis.

Dissolved Fe and pFe_{xs} showed positive linear relationships with fim (Fig. 6a, c with shelf stations excluded), indicating a clear flux from sea ice melt. However, the derived pure sea ice (fim = 1.0) end-member of these relationships of 2.35 nmol/kg for dFe and 27.5 nmol/kg for pFe_{xs} were on the low end of published sea ice estimates for Fe, which for Bering Shelf sea ice is 3–376 nmol/kg for dFe and 75–7,500 nmol/kg for total pFe (Aguilar-Islas et al., 2008). However, the dFe sea ice end-members is above the dFe range for GN01 central Arctic sea ice reported by Marsay et al. 2018 for GN01 (1.1 ± 1.0 nmol/kg; (Marsay et al., 2018)). Note that during the GN01 cruise, we did not see any visual evidence of "dirty ice", which might account for our low sea ice dFe values, relative to those in previous studies.

These results highlight the fact that while there is a sea ice source inferred for dFe and pFe on the basis of their linear relationships with fim, the sea ice contribution to dFe and pFe_{xs} inventories in surface waters appears to be small during the late summer, especially in contrast to the large fluxes from the continental shelf nearby (Fig. 6, open

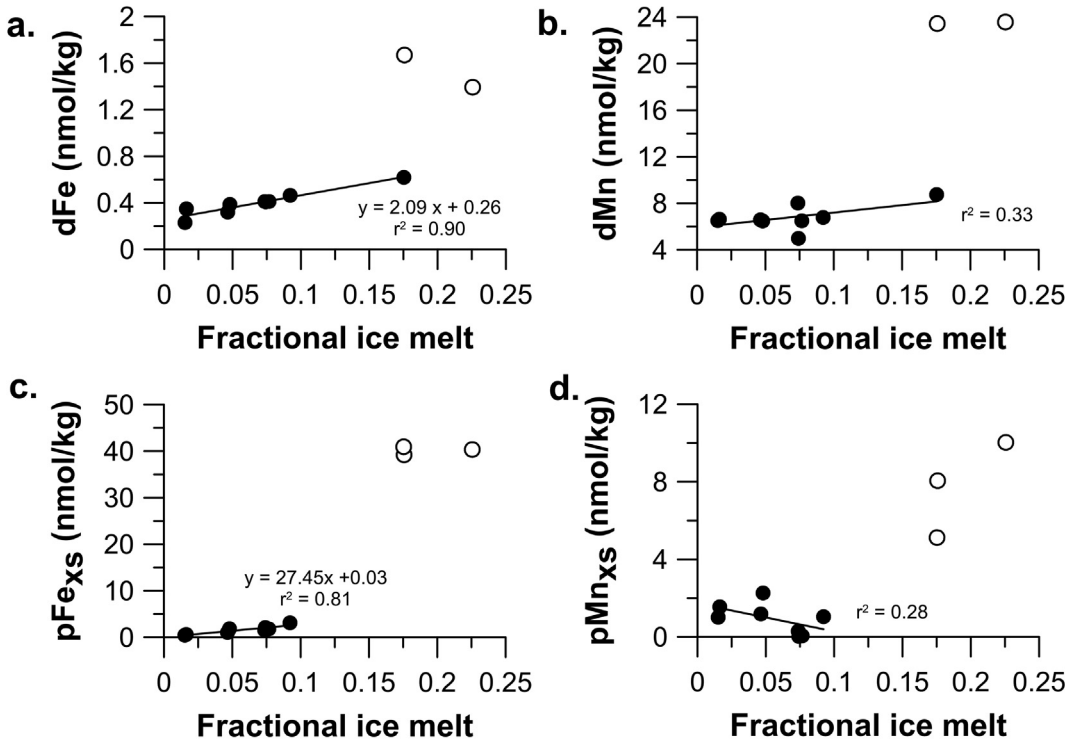

Fig. 6. Plots of (a) dissolved Fe, (b) dissolved Mn, (c) particulate Fe excess, and (d) particulate Mn excess in the surface at MIZ stations (8–17, 51–57) against fractional ice melt (fim = melted sea ice water/total water present from all sources). Stations 8–9 (Fe, Mn) or 8–10 (pFe_{xs}, pMn_{xs}) (open circles) have high shelf influence and values that fall outside the range of the other stations (12–17, 51–57, closed circles) and were therefore omitted from the regression.

symbols). We also note that while the mostly linear relationships ($r^2 = 0.90$ and 0.81 for dFe and pFe_{xs}, respectively) between Fe phases and fim indicate a relatively conserved source from sea ice, our narrow observed fim range of 2.5–17.5% ice melt cannot rule out curvature in these trends over a wider fim range, which might result from biological uptake, scavenging of the dFe, or aggregative sinking losses of the pFe. In contrast to Fe, dMn and pMn_{xs} did not have linear correlations with fim (Fig. 6b, d; $r^2 = 0.33$ and 0.28, respectively) likely due to overwhelming Mn inputs on the shelf. Thus, it appears that dissolved and excess particulate Fe were sourced from sea ice to the MIZ during GN01, based on this correlation, while dMn and pMn_{xs} had high shelf fluxes that overwhelmed any potential Mn supply to MIZ waters from sea ice.

3.2.2. Relationship to nutrients and other metals

Since dissolved Fe is an essential micronutrient for phytoplankton (Bruland and Lohan, 2003), we might expect that dFe would exhibit some correlation with other nutrients, particularly in the upper 400 m where biological cycling may have an influence. There are no strong correlations between dFe and nitrate ($r^2 = 0.34$) on the shelf (Fig. S3a), indicating that biological processes alone cannot explain the dFe distribution. On the shelf, there is a weak correlation between silicate and dFe that is driven by high concentrations in the deepest shelf samples ($r^2 = 0.60$, yellow circles, Fig. S2a), which could be explained by porewater fluxes of both silicate and dFe. In contrast, dMn and dFe are more strongly correlated ($r^2 = 0.64$) over the shelf (yellow circles, Fig. S2c), highlighting a common source that appears to overwhelm any water column biological processes on the shelf. Dissolved Fe and pFe_{xs} are also well correlated along the shelf ($r^2 = 0.76$, Fig. S2d) and within the UHL ($r^2 = 0.95$, Fig. S2d), although dMn and pMn_{xs} are not (Fig. S2e).

However, within the UHL, dFe showed a very low ($r^2 < 0.10$) correlation to any of the major macronutrients (Fig. S3). Even silicate, a well-known tracer of UHL waters (Anderson et al., 2013) where dFe is also elevated (Fig. 3), showed no strong correlation to Fe within the UHL (red circles in Fig. S2a). Away from the shelf in the UHL, we found that neither Fe nor Mn correlated with any major macronutrient in this study (Fig. S3), but they continued to be correlated with each other throughout the UHL ($r^2 = 0.85$), indicating their common shelf source.

Given this low correlation to biologically-cycled macronutrients, there is little evidence of *in situ* remineralization fluxes of dFe and dMn to offshore GN01 sites, likely resulting from low primary production under the sea ice at this time of year. The Arctic biological carbon pump is thought to have very low efficiency, given the low particulate organic carbon flux and lack of ^{234}Th deficiency offshore along these sites (Black, 2018), as well as low chlorophyll *a* (<150 ng/L) in the upper 100 m that is suggestive of oligotrophic conditions (Fig. 4e). This inference of

low remineralization supply is further bolstered by the fact that profile shapes for many metals and macronutrients (e.g. for dissolved zinc in Jensen et al. (2019)) do not match the classic "nutrient-type" curves. Instead, the Arctic appears to be dominated by large lateral fluxes of metals from the wide Arctic shelves. This confirms that the Western Arctic behaves as a useful template with which to examine dFe and dMn redox and transport behaviors, without overprinting by significant vertical biological fluxes.

In fact, the low chlorophyll *a* observed along GN01 basin stations (Whitmore et al., 2019) coupled with low surface dFe offshore in the central Canadian and Makarov basins could be indicative of Fe limitation of surface primary producers. Recent work in the Eastern Arctic demonstrated the potential for Fe limitation in the Nansen Basin where surface dFe concentrations are very low (Rijkenberg et al., 2018). Rijkenberg et al. (2018) used the tracer Fe* (Fe* = [dFe] – (Fe:N) × [N]) to evaluate the stoichiometric potential for Fe limitation, where Fe* < 0 suggests possible Fe limitation, and Fe:N is the biological uptake ratio of Fe to nitrate ($N = [NO_3^-]$). They defined two scenarios using different cellular ratios of Fe:P measured in Southern Ocean phytoplankton and converted those to Fe:N using the N:P ratio from the water column at their study sites. Following this same procedure using their two scenarios of Fe stress/limitation, we conclude that there is no current stoichiometric Fe limitation along the upper 100 m of the Canada and Makarov basins (Fig. S4). This is supported by relatively high Fe:P ratios measured in cells along GN01, suggesting that Fe uptake by phytoplankton cells is not restricted, as would be expected under Fe stress (Twining et al., 2017). However, we cannot discount possible future Fe stress in surface waters of the Canada Basin (Stations 14–26 and 46–57), where Fe* is closest to zero (<0.4) when calculated using the more Fe-rich cellular stoichiometry of Rijkenberg et al. (2018). Such a situation has been proposed in the Labrador Sea (Colombo et al., 2020).

3.3. Oxidation differences between Fe and Mn along the Bering and Chukchi shelves

The Chukchi Shelf and its influence on the UHL is the most obvious dissolved metal feature in the Western Arctic Ocean (Fig. 3), particularly within the Canada Basin (Aguilar-Islas et al., 2013; Cid et al., 2012; Colombo et al., 2020; Jensen et al., 2019; Kondo et al., 2016; Nishimura et al., 2012). The highest concentrations of dFe, pFe_{xs} and dMn in this study were found in the bottom waters along the Shelf and Strait stations (stations 61–66 and 2–8, respectively, Fig. 7), indicating a source from the sediments. This could occur from resuspension of sediments themselves (Vieira et al., 2019) or from authigenic reactions related to the biogeochemistry of porewater diagenesis (Burdige, 2006; Froelich et al., 1979). The Chukchi Shelf not only receives nutrient-rich inflow from the North Pacific via the Bering Strait (Aagaard et al., 1981), but it is also highly productive (Sakshaug, 2004).

In order to distinguish sediment resuspension from porewater diagenetic fluxes, we employed the porewater tracer N*, as used in previous studies of the region.. In those studies, N* (N* = (0.87[DIN]–16[PO_4^{3-}] + 2.9) μmol/kg) was employed as an ideal tracer of porewater diagenesis because it indicates the presence of denitrification, and water column denitrification over the Chukchi Shelf is unlikely given high water column oxygen concentrations (Aguilar-Islas et al., 2013; Granger et al., 2018; Nishino et al., 2005); thus, the low N* can only be produced in porewaters. The strong negative correlation between N* and dFe, dMn, and pFe_{xs} along the shelf (Fig. 8) confirmed a common authigenic porewater source for these metals, manifested as concentration maxima at the deepest sampled depths of the Chukchi Shelf stations (Fig. 7).

In contrast, pMn_{xs} remained low over the Chukchi Shelf and lacked a correlation to dFe, pFe_{xs}, or even dMn, which highlights our first major divergence in Fe and Mn distributions, specifically that Chukchi Shelf dMn concentrations were much higher than dFe (dMn ≫ dFe) but particulate excess Fe concentrations were much higher than particulate excess Mn ($pFe_{xs} \gg pMn_{xs}$) (Fig. S5). This disparity agreed well with data from the total particulate phase (Xiang and Lam, 2020). Studies in Arctic sediments in the Barents Sea, known to be second in primary production only to the Chukchi Sea (Sakshaug, 2004), have demonstrated that reduction of Fe(III) and Mn(IV) account for greater than 90% of the organic carbon oxidation (Vandieken et al., 2006). Thus, our first-order hypothesis would be a large, concurrent Fe and Mn diagenetic flux from Chukchi Shelf porewaters, up to 2.5 μmol/m^2/day for dFe and 8.0 μmol/m^2/day for dMn (Vieira et al., 2019), which is also supported by large Fe and Mn oxide abundances in the shelf and slope sediments (Hein et al., 2017; Trefry et al., 2014).

We observed that dFe and dMn were both enriched in near-bottom waters of the Chukchi Shelf (Fig. 7, Fig. S5), but dMn values were significantly higher (dFe ≪ dMn). While thermodynamics might favor the production of both within sediment porewaters, kinetics favors the rapid oxidation of Fe(II)/Fe(III) back to particulate Fe(III) in the presence of oxygen. This oxidation is known to be rapid, with a half-life on the order of minutes for typical seawater (Millero et al., 1987), but can be hindered by organic ligand complexation (Rue and Bruland, 1995). In contrast, Mn (II)/Mn(III) oxidizes much more slowly in the presence of oxygen (von Langen et al., 1997; Yeats and Strain, 1990), and its oxidation is often microbially-mediated (Nealson et al., 1988; Tebo et al., 2004), leading to a half-life on the order of days to weeks under typical seawater conditions (Stumm and Morgan, 1981).

We use the parameterization laid out in Millero et al. (1987) to calculate the half-life of Fe(II) along the Chukchi Shelf, where oxygen is variable (214–390 μmol/kg) as well as pH (7.21–7.92, (Kadko et al., 2016)), and *in situ* temperature, salinity, and pressure are used to calculate non-ideal equilibrium constants, yielding Fe(II) half-lives ranging from 35.8 minutes to 10.1 days (Fig. S6). Assuming a bottom water transport of 15–100 cm/s (Aagaard and Roach, 1990; Münchow and Carmack, 1997), we can estimate that the highly soluble Fe(II) could be transported 322 m to 883 km from its source before being diminished to half its original concentration. In fact, Fe (II) concentrations on

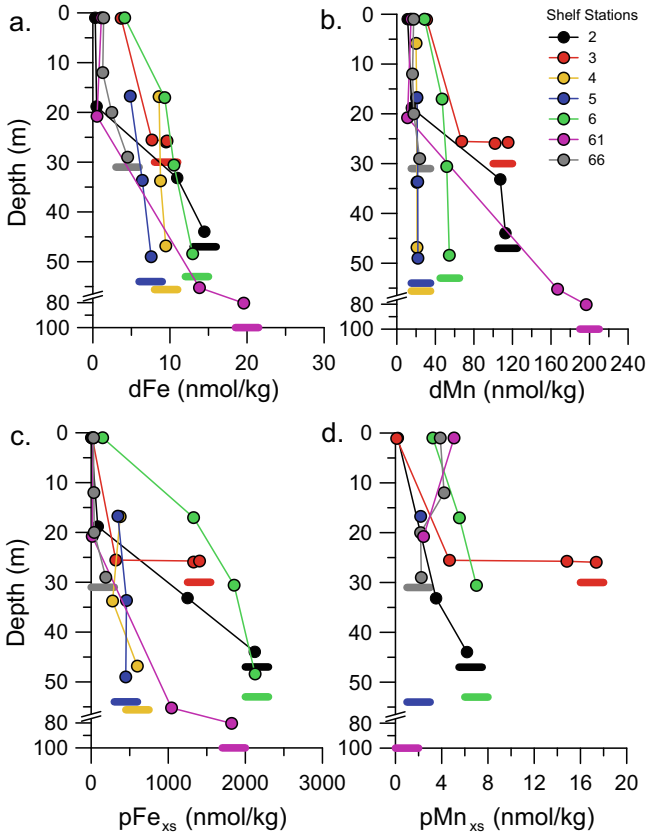

Fig. 7. Bering Strait/Chukchi Shelf station profiles of (a) dFe, (b) dMn, (c) pFe$_{xs}$, (d) pMn$_{xs}$ to show full range of elements at these important stations. The bottom depth for each station is shown as a solid bar below the plot to illustrate how close sampling depth was to "true bottom" along the Chukchi Shelf.

the shelf were generally quite low (<15 pmol/kg), composing at most 2.5% of the overall dissolved phase (Fig. S7). This suggests that most of the dFe is Fe(III), in the form of either Fe oxyhydroxide nanoparticles or Fe(III)-organic ligand complexes. In contrast, the half-life of Mn (II) oxidation, calculated following Yeats and Strain (1990) as a function of pH, oxygen, and particulate Mn concentration, ranges 700 minutes to 41.3 days and can be transported between 6.3 and 3600 km away from its source before significant oxidation and removal. This suggests that any Fe(II) released during porewater diagenetic reactions was more rapidly oxidized to nanoparticulate and especially particulate phase (Fe(III)), while Mn(II) remained in the dissolved phase much longer.

3.3.1. Offshore transport of Fe and Mn in the UHL

The elevated concentrations of dFe, pFe$_{xs}$, and dMn on the Chukchi shelves were also maintained within the UHL (Figs. 3 and 4). Due to brine rejection associated with sea ice formation on the Chukchi Shelf, nutrient- and metal-rich waters are subducted and transported offshore, creating a highly traceable water mass characterized by elevated Si concentrations ([Si] > 25 µmol/kg, (Anderson et al., 2013)) (Fig. 3). While dMn remained elevated in surface waters (Fig. 4), likely due to a slow oxidation timescale after advection from the continental shelves and/or surface photoreduction of Mn oxide particles into dissolved Mn(II) away from sea ice coverage (Sunda et al., 1983; Sunda and Huntsman, 1994), dissolved Fe and Mn both had their local maxima in offshore waters within the UHL (Fig. 3). Maxima in dFe, dMn, and Si were all maintained throughout the Canada Basin UHL (Stations 8–19, 46–60), extending hundreds of kilometers away from the Chukchi Shelf, as observed in recent studies, albeit with lower concentration ranges (Colombo et al., 2020). While UHL waters were not circulated directly northward along our cruise transect and instead can be entrained within cyclonic circulation along coastal currents at certain latitudes (Rudels, 2015), it is useful to consider mechanisms affecting this long-range transport of shelf-derived Fe and Mn offshore and compare to other studies that have considered Fe and Mn transport length scales.

How long might we expect various Fe and Mn species to persist over distance, based on prior studies? As calculated above, we know that the reduced forms of dissolved Fe and Mn are oxidized on different timescales, and that the oxidized species are nearly quantitatively removed back into the (nano)particulate phase, effectively removing them from the water column. However, dissolved Fe(III), the thermodynamically stable form of dissolved Fe in oxygenated waters (Kuma et al., 1996), is highly complexed by organic ligands in all oceanic waters (>99%, (Gledhill and Buck,

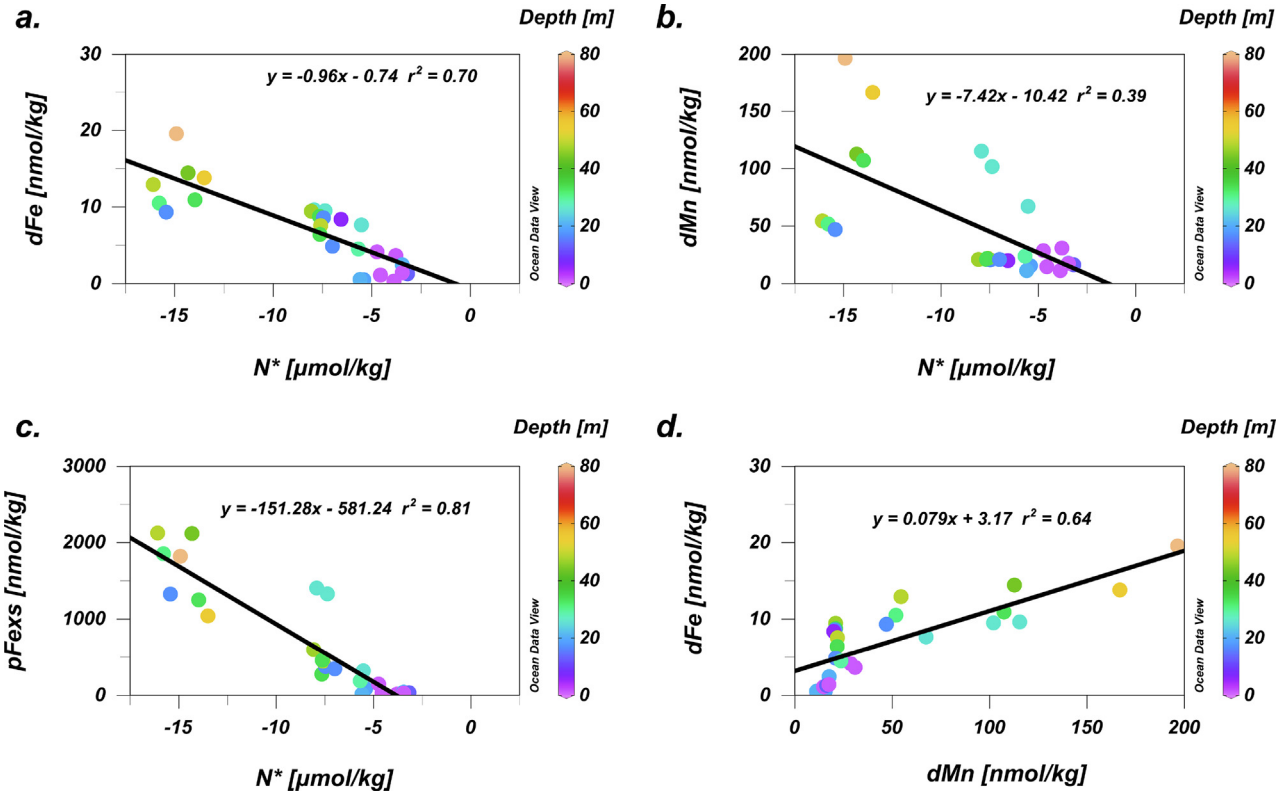

Fig. 8. (a) dFe, (b) dMn, (c) pFexs, along the shelf and strait (Stations 2–6, 61, 66) vs. the tracer of porewater denitrification N*. Panel (d) shows dFe vs dMn along the same stations demonstrating strong correlation. Depths of samples (0–80 m) are displayed in color showing that in most cases, the relationship is driven by benthic processes.

2012)). In contrast, Mn(II) generally remains as the ionic dissolved Mn^{2+} species (Tebo, 1991), though contribution by dissolved Mn(III) phases, which can be complexed organically, is also possible (Luther et al., 2015; Oldham et al., 2017) but unstudied in the Arctic. Without Fe ligand data available from the Western Arctic, we rely on previous studies in the Eastern Arctic Ocean and North Pacific demonstrating the guiding role of humic-like ligands in complexing and stabilizing dFe (Hioki et al., 2014; Slagter et al., 2019, 2017; Yamashita et al., 2020). Given the persistence of humic organic matter within the halocline (Hioki et al., 2014; Slagter et al., 2019, 2017; Yamashita et al., 2020), we can hypothesize that organic ligands are binding and stabilizing dFe in the halocline, making it less susceptible to adsorptive scavenging following oxidation (Gledhill and Buck, 2012; Tagliabue et al., 2017), while dMn is mostly present as free ionic Mn^{2+} or is at most partially stabilized by organic ligands as Mn(III). Thus, we might hypothesize that ligand stabilization could increase the longevity of dFe transport offshore relative to dMn, despite faster oxidation kinetics of the initial Fe(II) diagenetic flux.

One metric used to assess the lifetime of a margin-derived element is the natural log-scale transport (here defined as d_{ln}) of a species away from the continental shelf, which is the distance traveled offshore from the continental shelf before the element's concentration is reduced by 1/e of the original shelf concentration (Johnson et al., 1997). In the Arctic, this was first used in a study comparing the longevity of pFe and dFe from the Chukchi Shelf (Aguilar-Islas et al., 2013), demonstrating that within the Canada Basin UHL, pFe was removed more quickly (over shorter distances) than dFe (260 km compared to 380 km). Concentrations appeared to decrease exponentially offshore, leading to a simple linearization of the natural log of concentration versus distance from the shelf-break. We applied the same equation used in Aguilar-Islas et al. (2013) to all GN01 data that fall within the bounds of the UHL (S ~ 31–33.1, [Si] > 25 µmol/kg), representing a longer total distance (0–1200 km) from the shelf break, defined here as the 100 m isobath along the Chukchi Shelf, north of the shelf-break and slope currents (Corlett and Pickart, 2017).

We would expect that if chemical species were conserved in the UHL that a plot of natural log vs. distance from the shelf break would show a flat horizontal line. For example, ln(Si) vs. distance yields a horizontal line (Fig. 9g), suggesting that Si concentrations barely change in the halocline with distance from the shelf. Thus, a conserved element like Si is not being supplied significantly to the UHL by *in situ* regeneration nor significantly diluted by mixing with non-halocline waters (which have lower Si concentrations). This supports our case that the UHL is a useful layer in which to quantify scavenging length scales in the absence of overprinting by other oceanographic processes.

In contrast to Si, ln(dFe) vs. distance had a non-horizontal, linear decrease moving offshore (Fig. 9a), pointing to removal of Fe away from its shelf source. Similarly, we found linear relationships for ln(dMn) and ln(pFe_{xs}) vs. distance, also indicative of removal within the halocline (summarized in Table 2, Fig. 9). However, in contrast to the Aguilar-Islas et al. (2013) conclusions, we noticed two distinct slopes across 1200 km of transport: a rapid attenuation of dFe, dMn, and pFe_{xs} within 150 km of the shelf break, followed by slow removal of dFe and pFe_{xs} and conservation of dMn between 150 and 1200 km. Within 150 km of the shelf break, d_{ln} was only 74 ± 1 km for dFe, which is a much shorter scavenging removal distance than the Aguilar-Islas estimate of 380 km (Table 2). Dissolved Mn and pFe_{xs} were removed even faster, with a d_{ln} of approximately 40 km (Table 2). Farther offshore at 150–1200 km from the shelf break, d_{ln} for dFe increased to 2,051 ± 613 km, indicating much slower scavenging, and pFe_{xs} had a d_{ln} of 770 ± 384 km, again persisting much farther, while the natural log of dMn shared no statistically significant relationship ($r^2 < 0.2$) with distance from the shelf break (Fig. 9). We compared the initial d_{ln} distances for dFe and pFe_{xs}, which were shorter than those found previously in the Arctic and shorter than most other reported values (Table 2), and noted two major conclusions. First, this multi-step removal process was not reported in prior similar studies, even in the Arctic. Second, dFe was stabilized farther than dMn at first, but dFe was subject to slow removal across the longer 1200 km offshore spatial scale, whereas dMn was conserved after initial scavenging losses near the shelf break.

Dissolved Fe, as previously mentioned, can be highly organically complexed in marine waters, which is thought to protect it from scavenging to the particulate phase (Gledhill and Buck, 2012; Rue and Bruland, 1995). Particulate Fe (pFe_{xs} in this study) was more rapidly diminished, likely falling out of the water column due to aggregation. Likewise, dMn was eventually oxidized to pMn_{xs}, which appears to "grow in" within the halocline offshore despite dMn being conserved (Figs. 3d and 9d). Close to the shelf, dFe and dMn have very different spatial scales of removal, likely demonstrating the stabilizing effect of ligands on dFe. Despite this, dFe still appeared to be removed offshore, presumably over longer timescales and distances, even farther than the d_{ln} recently reported within Arctic waters transiting Canadian Archipelago to the Davis Strait (~1450 km, (Colombo et al., 2020)). Dissolved Mn, in contrast, was conserved in these same offshore waters. To further investigate the speciation of dFe and dMn that might cause these patterns, in the absence of ligand measurements, we examined the colloidal size distribution of dFe.

Colloidal Fe, an intermediate size fraction between truly soluble and larger particulate phases (Wells, 2002), is gaining increased attention as a size class of Fe than can drive enrichments of dFe close to continental sources (Bergquist et al., 2007; Fitzsimmons and Boyle, 2014b; Fitzsimmons et al., 2015). This study represents the first basin-scale section of size-fractionated dFe in the Arctic. In the North Atlantic, soluble Fe concentrations (sFe < 0.02 μm) matched colloidal Fe (cFe) concentrations (~50% sFe or cFe), except at margin- and hydrothermal-influenced depths where colloids dominated (cFe > 50%; Fig. 10) (Fitzsimmons et al., 2015). In contrast, the Arctic was instead dominated by soluble Fe species (only 25 ± 16% cFe; Fig. 10), despite similar dFe concentrations as the North Atlantic. This was surprising, given the significant margin-influence in the Arctic Ocean and the high particulate Fe concentrations, which might be expected to correspond to higher nanoparticle concentrations that are often observed in the colloidal size fraction. However, even within the halocline close to the shelf, %cFe was only 21 ± 15%. Extending our previous log-scale transport calculations to these size-fractionated dFe species, the d_{ln} for sFe was 152 ± 64 km (Fig. 9e, Table 2), while colloidal Fe (cFe) had a much shorter d_{ln} of 34 ± 2 km (Fig. 9f). This suggests that cFe was scavenged nearly 5 times as rapidly as sFe close to the shelf. In the second, longer-distance scavenging regime, sFe had a log scale transport of 2400 ± 742 km, and cFe surprisingly appeared conserved. Dissolved Mn was entirely soluble-sized in the Arctic, with 0 ± 7% of dMn falling into the colloidal size fraction.

Size partitioning of dFe phases does not clarify the chemical composition of dFe, as both ligand-bound Fe and inorganic Fe nanoparticles can be observed in both the soluble and colloidal size fractions. However, the soluble-colloidal log-scale transport pattern could be interpreted as a greater presence of stable Fe bound by organic ligands within the soluble size fraction near the shelf, with actively aggregating nanoparticles contributing more to the shorter lived colloidal size fraction. Overall, the starkly lower concentration of colloids across the entire Western Arctic transect compared to the North Atlantic marks a major change in the speciation of dFe in these two ocean basins. In the absence of other Fe speciation data, we can only speculate on the cause of this difference, which may be related to lower dust inputs to the Arctic providing fewer Fe colloids, or less biological productivity in overlying waters that would otherwise promote dFe transfer to the colloidal phase. Perhaps most compelling is the role of greater particle loads and more metal-rich particles in the Arctic, particularly on the shelf where Fe colloids were elevated (%cFe = 65 ± 22%), which could remove colloids faster in the Arctic than in other ocean basins.

4. BIOGEOCHEMICAL IMPLICATIONS AND FRAMEWORK

The Arctic Ocean provides an excellent model system with which to compare and contrast Fe and Mn chemistry. Despite a geochemical tendency to consider Fe and Mn as cycling together because of broadly common sources and sinks (Fig. 1), their chemical behavior and speciation and thus reactivity are different and lead to decoupled distributions within the upper 400 m of the Western Arctic Ocean. In the relative absence of overprinting from external fluxes or biological transformations, we present a relatively simple demonstration of the contrasting oxidation rates and scavenging of Fe and Mn within the water column.

Our results show a three-step differentiation of the Fe and Mn distributions in the Arctic. First, there is a large,

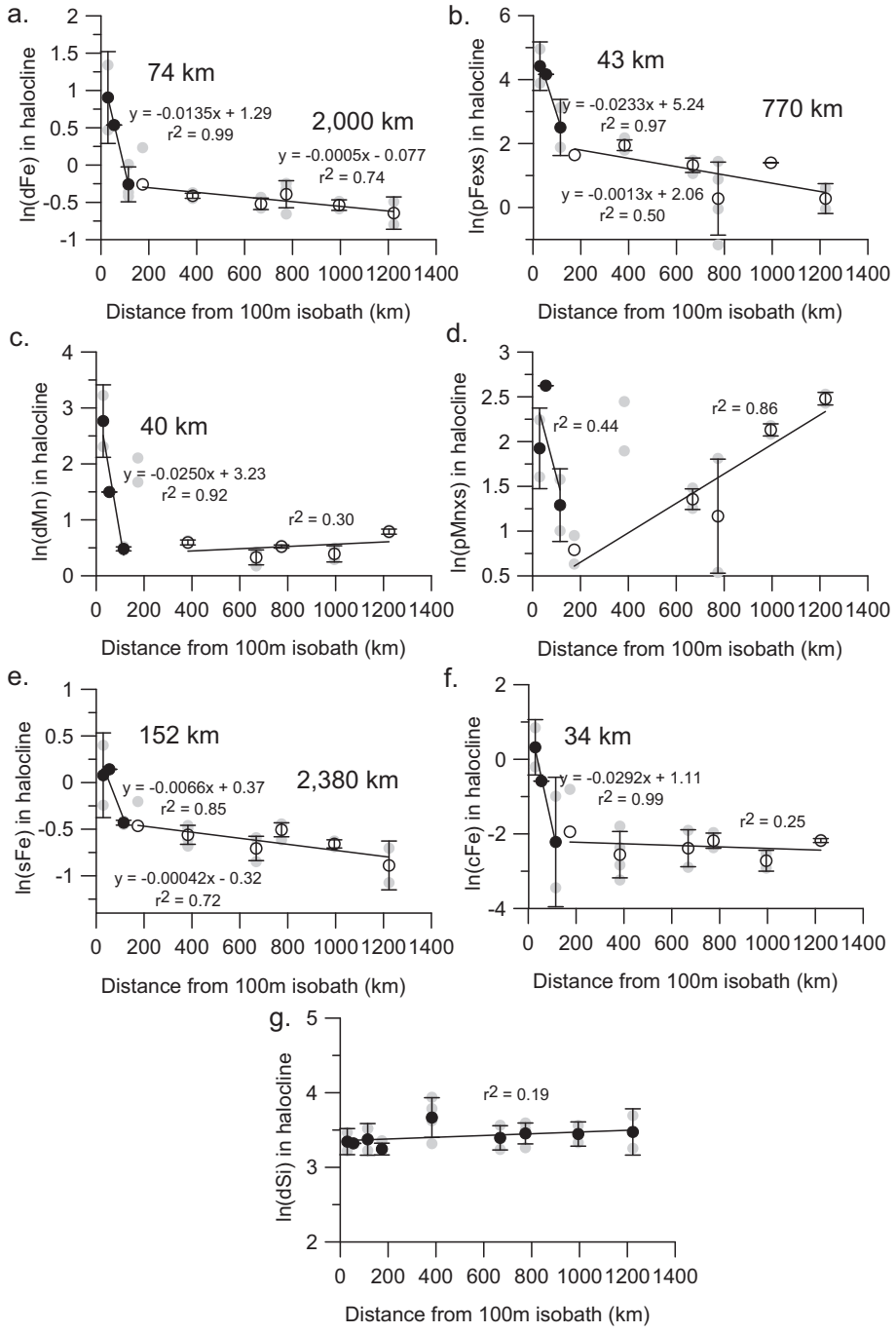

Fig. 9. Log-scale transport plots of ln([metal]) vs. distance from the 100 m isobath along the Chukchi Shelf for Stations 8, 10, 14, 19, 46, 48, 52, 57, and 60 in the Canada Basin. All data (grey circles) are taken within the bounds of the upper halocline as defined by silicate concentration ([Si] = 25 μmol/kg) and salinity 31.0–33.1. Averages for each station are represented by filled circles (close to shore, Stations 8, 57, 60) or open circles (further from shore, Stations 10, 14, 19, 52, 46, 48) to show the general trend with accompanying error bars. Linear regression equations are shown for significant relationships. The d_{ln} values (1/slope, distance over which variable decreases by 1/e) are shown in bold where relationship is statistically significant (r2 > 0.5) and mentioned in the text. (a) dFe, (b) pFexs, (c) dMn, (d) pMnxs, (e) sFe, (f) cFe, (g) silicate.

diagenetic porewater flux that releases both dFe and dMn via reductive dissolution of Fe and Mn oxides in Chukchi Shelf sediments. However, the two metals are immediately decoupled at their source, when faster oxidation kinetics of Fe(II) in the presence of oxygen creates high pFe_{xs} (up to 2100 nmol/kg) compared to dFe (up to 19.6 nmol/kg), and slower oxidation of Mn(II) allows for high dMn (up to 196 nmol/kg) and lower pMn_{xs} (up to 17 nmol/kg).

Table 2
Summary of log scale transport distance (d_{ln} in km) values for this study (bold) compared to literature values. Studies are generally listed in increasing order of dFe d_{ln} distance, with location and depth noted where possible. The double values reported for this study indicates that two distinct linear relationships were found, one closer to the shelf and one farther offshore, leading to two d_{ln} values. Associated errors in d_{ln} (1SD, derived from the linear regression) are reported for this study only.

Reference	Location	Depth	dFe		pFexs		sFe		cFe		dMn	
Johnson et al. (1997)	Monterey Bay	Surface	16		–		–		–		–	
This study	**Canada basin**	**100–200**	**74 ± 1**	**2051 ± 613**	**43 ± 8**	**770 ± 384**	**152 ± 64**	**2400 ± 742**	**34 ± 2**	–	**40 ± 12**	–
Wu and Luther (1996)	Delaware Bay	–	101		–		–		–		–	
Gordon et al. (1998)	Galapagos	–	103		–		–		–		–	
Bucciarelli et al. (2001)	Kerguelen	Surface	151		–		–		–		–	
Klunder et al. (2012a, 2012b)	Nansen basin	750	260		–		–		–		–	
Aguilar-Islas et al. (2013)	Canada Basin	200–250	380		260		–		–		–	
Johnson et al. (1997)	Coastal CA	1000	5000		–		–		–		–	

These patterns confirm rapid Fe oxidation and slower (kinetically inhibited) oxidation of Mn (Stumm and Morgan, 1981; von Langen et al., 1997; Yeats and Strain, 1990). We might expect that this Fe:Mn pattern would persist moving offshore into the shelf-influenced UHL. However, the second step of Fe and Mn differentiation occurs within the UHL < 150 km from the shelf, where there is rapid removal of both dFe and dMn (Fig. 9). Then, in the third step of differentiation even farther offshore (>150 km from shelf break), dFe persists with very slow scavenging, likely due to the presence of soluble-sized organic ligands that allow soluble Fe to have a longer d_{ln} than any other species. In contrast, dMn is more rapidly removed to the particulate phase in the near-shelf scavenging regime, in line with previous work along the Chukchi slope and basin (Macdonald and Gobeil, 2012), but remains conserved through the next 1000 km away from the shelf.

This three-step Fe and Mn differentiation explains the overall balance of the dissolved and particulate phases of Fe and Mn. Much of the dissolved Fe is converted to particulate Fe immediately over the shelf, and some of this particulate Fe persists offshore. In contrast, dissolved Mn persists over the shelf without precipitating but is eventually transformed to pMn within the halocline (Figs. 3d and 9d). The particulate phase eventually dominates for both metals below 100 m, which isn't necessarily true in the rest of the global ocean where dMn often dominates pMn and dFe ≈ pFe at depth, e.g. (Noble et al., 2012), but this pattern is consistent with other studies in the Canada Basin and along the Bering and Chukchi shelves (Aguilar-Islas et al., 2013). The differentiation between the second and third steps can thus be ascribed to a zone of higher aggregation/scavenging on/near the shelf due to higher particle abundances and then a zone of lower removal offshore where Fe scavenging is mostly complete but some pMn formation is still occurring (Figs. 3f; 11). The origin of this pMn formation is unknown, but recent studies attribute it to either vertical fluxes from the relatively shallow Alpha-Mendeleev Ridge (~2200 m) separating the Makarov and Canada basins or (more likely) lateral advection from shelf sources that may not be adequately captured by our transect (Xiang and Lam, 2020). *In situ* oxidation of dMn to the particulate phase is not supported by our data, as dMn is conserved in the halocline at these stations.

This decoupling of Fe and Mn has been observed in prior studies from various oceanic regimes (Fitzsimmons et al., 2017; Hatta et al., 2013, 2015; Landing and Bruland, 1987; Noble et al., 2012). The basic nature of the three-step decoupling found in this study is mirrored in buoyant hydrothermal fluids (Step 1) and neutrally-buoyant plumes (Steps 2 nearer the vent and Step 3 farther from the vent). For example, in the Southern East Pacific Rise (SEPR) hydrothermal plume study of Fitzsimmons et al. (2017), the scavenging regimes and subsequent distributions of Fe and Mn were different, with dMn conserved down the plume and dFe both removed and found to deepen with sinking particles. Those authors concluded that a reversible scavenging between the dissolved and particulate Fe phases was necessary to explain the distributions, and they proposed an essential role of organic compounds in driving the Fe exchange. The SEPR study employed Fe isotopes to suggest that Fe oxyhydroxide nanoparticles were scavenged more rapidly than the ligand-bound dFe compounds, and that was used as a framework for the difference between Step 2 and Step 3 dFe loss observed here (Fig. 9).

In fact, the three-step differentiation proposed here both contradicts and supports our current understanding of residence time in the upper water column, namely that dFe is thought to be shorter-lived than dMn (Bruland et al., 1994; Landing and Bruland, 1987). Nearer to the shelf, dFe appears "longer-lived" than dMn, based on the longer d_{ln}, which is controlled primarily by the soluble phase (Fig. 9a, e, f). However, beyond this region of initial rapid removal, dFe, sFe, and pFe_{xs} are slowly removed and dMn remains conserved, as in the SEPR plume (Fitzsimmons et al. 2017). Offshore, it may be the pMn_{xs} that is responsible for scavenging of dFe and sFe far away from the shelf source (Cheize et al., 2019). The similar scavenging kinetics of pFe_{xs} and cFe in the Arctic can be explained if cFe in the Arctic were largely inorganic (nanoparticulate) in charac-

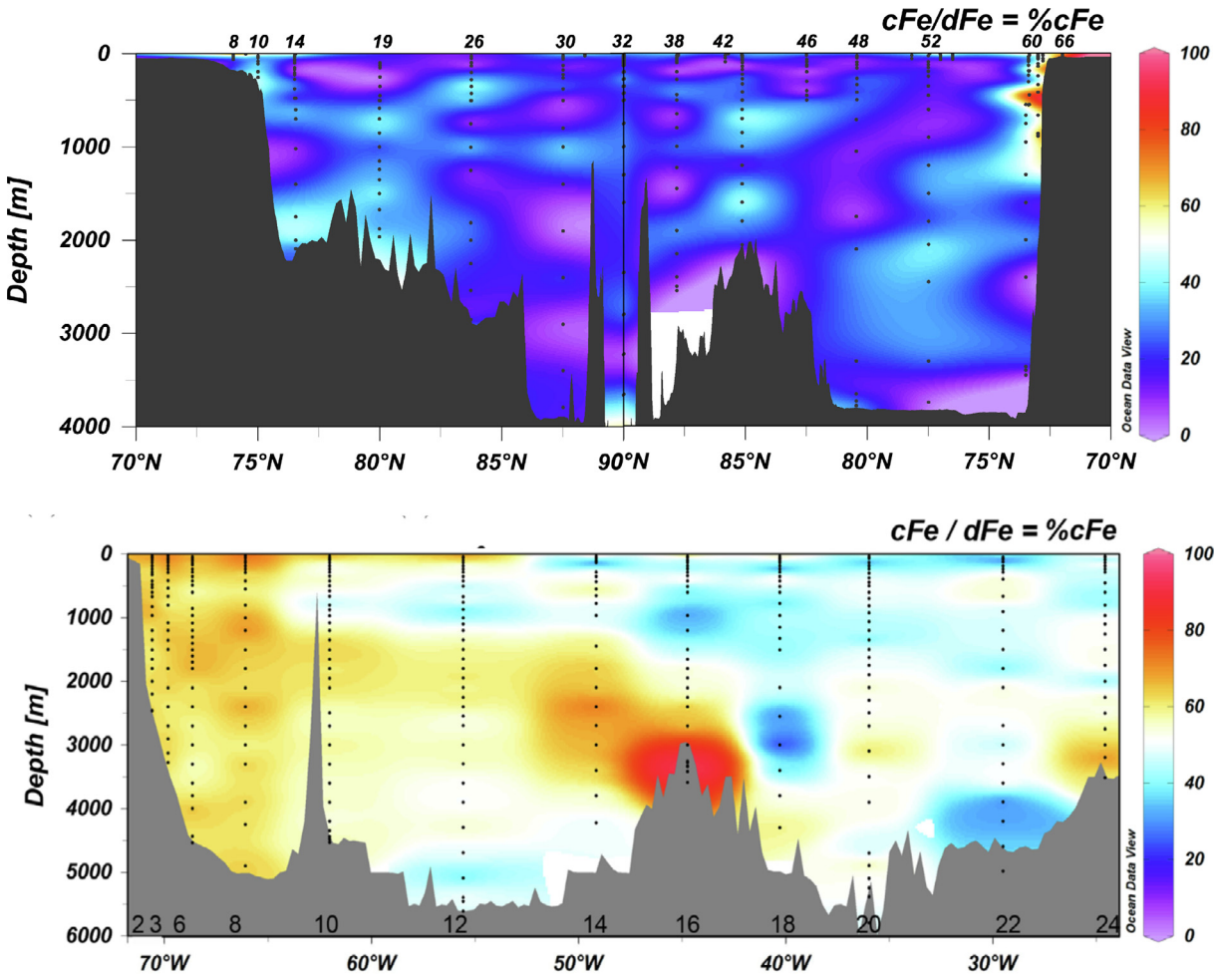

Fig. 10. Comparison of the Arctic Ocean (top, this study) with the North Atlantic (bottom, U.S. GEOTRACES GA03; Fitzsimmons et al., 2015). The color bar represents the %cFe or cFe/dFe × 100%. Notably, the Arctic Ocean overall contains a very low colloidal contribution (average %cFe = 25 ± 16%, 1SD) to the dissolved phase compared to the only other ocean basin section for which this quantity has been measured. Stations for this study only are shown at the top of the panel.

ter, leading to similar cFe aggregation and sinking from the water column as pFe_{xs}, as posited in Aguilar-Islas et al. (Aguilar-Islas et al.). However, farther offshore the cFe remains low and conserved, like dMn, indicating a different, perhaps organic, chemical composition of this offshore UHL cFe phase.

As the "Scavengers of the Sea" (Goldberg, 1954), the opposite distributions of particulate Fe oxides (over the shelf) and particulate Mn oxides (offshore in the halocline) will also affect the distributions of other scavenging-prone trace metals, both in the water column and in the sediments below. Previous studies have demonstrated that different elements have a tendency to sorb either to Fe oxyhydroxides (which are surface neutral or slightly positively charged) compared to Mn oxides (which have negatively charged surfaces), based on the dominant inorganic speciation of the dissolved trace elements (Koschinsky and Hein, 2003). For example, trace metals found in seawater as weakly complexed cations (Byrne, 2002), such as most rare earth elements, are expected to sorb more readily to Mn oxides, while negatively charged carbonate and chloride complexes such as Sc, Cu, Ti, Zn (Byrne, 2002) are more readily absorbed to Fe oxides (Koschinsky and Hein, 2003). Thus, we might expect this first group to have higher abundances in slope/offshore sediments, while the second group may have higher abundances in shelf and near-shelf sediments. A recent study found high Fe:Mn ratios in Fe-Mn nodules just off of the Chukchi Shelf, indicative of Fe being "shuttled" efficiently off of the shelf and precipitating as Fe oxyhydroxides (Hein et al., 2017). These so-called "Fe shuttles" have been described in margin sediments and in oxygen minimum zones (OMZ) elsewhere (Raiswell, 2011; Scholz et al., 2011) and may be responsible for moving other elements offshore (Whitmore et al., 2019).

5. CONCLUSIONS

Dissolved Fe and Mn share many common sources and sinks in the global ocean, such as release from sediments, dust fluxes, hydrothermal venting, biological uptake, and scavenging to the particulate phase. Despite multiple field investigations demonstrating their decoupling, many stud-

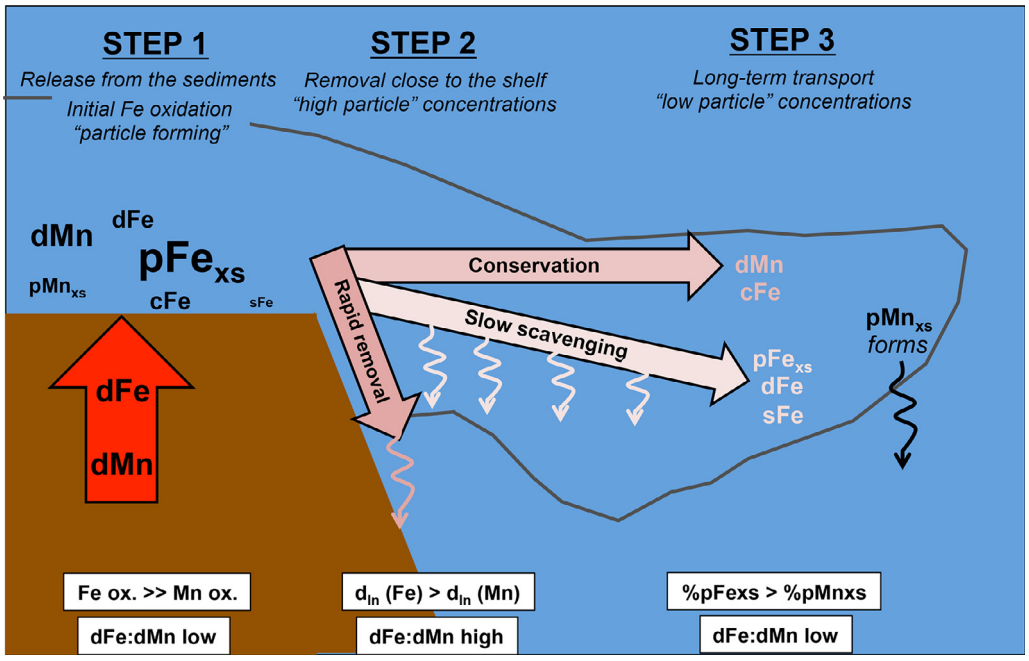

Fig. 11. Summary schematic of the major trends described in the text. A three-step differentiation pattern between Fe and Mn is clearly demonstrated by (1) unequal oxidation kinetics leading to particle formation on the shelf following by (2) rapid removal of both species close to the shelf and (3) continued removal of Fe while Mn remains conserved. The size of the text on the shelf indicates relative concentrations of various Fe and Mn species. Squiggly arrows indicate removal from the water column, likely leading to eventual burial in the sediments.

ies continue to compare the two to identify common e.g. hydrothermal or continental margin fluxes. The Western Arctic Ocean provided an ideal, simple case study for resolving how some of the chemical properties that differentiate Fe and Mn, such as the timescale of oxidation and stabilization by organic ligands, affect their distributions. Our results produced a three-step decoupling framework for Fe and Mn in both the dissolved and particulate phases from the shelf to offshore waters: the first step was the rapid loss of dFe to pFe_{xs} but maintenance of dMn following reductive dissimilation during the decay of organic matter in porewaters, while the second step occurred within the nearby high-particle waters where both dFe and dMn and also pFe_{xs} were all scavenged and aggregated, with only the smallest soluble Fe, likely dominated by strong organic ligand complexes, somewhat protected from this removal; and finally the third step of Fe and Mn differentiation was the continued slow removal of dFe, sFe, and pFe_{xs} within the UHL between 150 and 1200 km offshore, while dMn and cFe were net conserved, possibly due to an equilibrium of sources and sinks during offshore transport.

These three opportunities for Fe and Mn decoupling, based largely on differences in their oxidation kinetics and speciation, prevent Fe and Mn from sharing similar distributions in the global ocean, despite their similar sources and sinks. A correlation between Fe and Mn could indicate the presence of a shared source, such as hydrothermal venting, diagenetic fluxes (as seen in this study), or dust input to the surface ocean. However, a lack of correlation between the two metals does not prevent the identification of one of these shared supply mechanisms, as Fe or Mn may have been removed more than the other on various spatial scales due to these differentiation steps. The chemical properties of Fe and Mn that drive their unique reactivity and speciation, as examined here and in many prior studies, serve to decouple these two elements across temporal and spatial scales. Future studies should recognize the influence of Fe and Mn in both the dissolved and particulate phases on the distribution of other trace elements, especially in shelf-influenced oceanic margin regions.

We also mention here the implications of a changing climate for the distribution and influence of Fe and Mn in the Western Arctic Ocean. The Chukchi Shelf is prone to seasonal variation in both productivity and organic carbon export to the seafloor as a direct result of ice cover (Harrison and Cota, 1991; Hill and Cota, 2005; Lepore et al., 2007). These seasonal "pulses" of organic matter can instigate the intermittent dissimilatory reduction of Fe and Mn in Arctic sediments (Magen et al., 2011; Vandieken et al., 2006). Thus, we should expect that the temporal variability of Fe and Mn flux to the UHL from the shelf is a function not only of physical circulation processes but also of seasonal changes in organic matter export. Likewise, as sea ice coverage retreats annually with climate change, there has been a 30% increase in net primary productivity throughout the Arctic Ocean over just the last 14 years (Arrigo and van Dijken, 2015), necessarily leading to increased export of organic matter to the shelf seas where productivity is highest (Sakshaug, 2004). This will in turn increase the mobilization of redox-sensitive metals such as Fe and Mn, which will subsequently oxidize and may then increase the scavenging of other metals throughout the water column.

Declaration of Competing Interest

The authors declare that they have no known competing financial interests or personal relationships that could have appeared to influence the work reported in this paper.

ACKNOWLEDGEMENTS

We would like to thank the Captain and crew of the USCGC Healy, Dave Kadko and Greg Cutter for proposing and enabling cruise leadership, Sara Rauschenberg and GN01 Supertechnicians Gabi Weiss and Simone Moos for sample collection at sea, Luz Romero for assistance with ICP-MS analyses and maintenance, and Angelica Pasqualini, Bob Newton, Peter Schlosser and Tobias Koffman for contribution of their oxygen isotope measurements and freshwater model estimates. Additionally, this work would not have been possible without the SIO ODF team for salinity, dissolved oxygen, and macronutrient analyses and Ana Aguilar-Islas and Rob Rember for ice hole sampling for the community. Finally, we thank three anonymous reviewers for their comments that significantly improved this paper. This work was supported by NSF Division of Ocean Sciences (OCE) award 1434493 and 1713677 to JNF and RMS, NSF OCE 1436019 to PM, NSF OCE 1435862 to BST, NSF OCE 1540254 to SGJ, NSF-OCE 1439253 to CIM, and NSF OCE-1535854 to Phoebe Lam (UCSC) as support for MIH. The National High Magnetic Field Laboratory is supported by the National Science Foundation through DMR-1644779 and the State of Florida.

RESEARCH DATA

The temperature, salinity, and macronutrient data as well as dissolved and particulate iron and manganese concentrations can be found at the Biological and Chemical Oceanography Data Management Office (BCO-DMO) repository. These Research Data associated with this article can be accessed at: http://doi.org/10.1575/1912/bco-dmo.647259.4 (for temperature, salinity, and macronutrient data), http://doi.org/10.26008/1912/bco-dmo.817259.1 (for dissolved metals), https://doi.org/10.1575/1912/bco-dmo.771474.2 (for particulate metals), and https://doi.org/10.26008/1912/bco-dmo.811614.1 (for Fe(II) data). Stable oxygen isotope data used in this work can be found through EarthChem Library: https://doi.org/10.1594/IEDA/100633.

APPENDIX A. SUPPLEMENTARY MATERIAL

Supplementary data to this article can be found online at https://doi.org/10.1016/j.gca.2020.08.006.

REFERENCES

Aagaard K., Coachman L. and Carmack E. (1981) On the halocline of the Arctic Ocean. *Deep Sea Res. Part A Oceanogr. Res. Pap.* **28**, 529–545.

Aagaard K. and Roach A. (1990) Arctic ocean-shelf exchange: Measurements in Barrow Canyon. *J. Geophys. Res. Oceans* **95**, 18163–18175.

Aagaard K., Swift J. H. and Carmack E. C. (1985) Thermohaline circulation in the Arctic Mediterranean Seas. *J. Geophys. Res. Oceans* **90**, 4833–4846.

Aguilar-Islas A. M., Rember R., Nishino S., Kikuchi T. and Itoh M. (2013) Partitioning and lateral transport of iron to the Canada Basin. *Polar Sci.* **7**, 82–99.

Aguilar-Islas A. M., Rember R. D., Mordy C. W. and Wu J. (2008) Sea ice-derived dissolved iron and its potential influence on the spring algal bloom in the Bering Sea. *Geophys. Res. Lett.* **35**.

Anderson L. G., Andersson P. S., Björk G., Peter Jones E., Jutterström S. and Wåhlström I. (2013) Source and formation of the upper halocline of the Arctic Ocean. *J. Geophys. Res. Oceans* **118**, 410–421.

Arimoto R., Duce R., Ray B. and Unni C. (1985) Atmospheric trace elements at Enewetak Atoll: 2. Transport to the ocean by wet and dry deposition. *J. Geophys. Res.: Atmos.* **90**, 2391–2408.

Arrigo K. R., Perovich D. K., Pickart R. S., Brown Z. W., van Dijken G. L., Lowry K. E., Mills M. M., Palmer M. A., Balch W. M., Bahr F., Bates N. R., Benitez-Nelson C., Bowler B., Brownlee E., Ehn J. K., Frey K. E., Garley R., Laney S. R., Lubelczyk L., Mathis J., Matsuoka A., Mitchell B. G., Moore G. W. K., Ortega-Retuerta E., Pal S., Polashenski C. M., Reynolds R. A., Schieber B., Sosik H. M., Stephens M. and Swift J. H. (2012) Massive phytoplankton blooms under Arctic Sea Ice. *Science*.

Arrigo K. R. and van Dijken G. L. (2015) Continued increases in Arctic Ocean primary production. *Prog. Oceanogr.* **136**, 60–70.

Balistrieri L., Brewer P. and Murray J. (1981) Scavenging residence times of trace metals and surface chemistry of sinking particles in the deep ocean. *Deep Sea Res. Part A Oceanogr. Res. Pap.* **28**, 101–121.

Barbeau K., Rue E. L., Bruland K. W. and Butler A. (2001) Photochemical cycling of iron in the surface ocean mediated by microbial iron(iii)-binding ligands. *Nature* **413**, 409–413.

Bergquist B. A., Wu J. and Boyle E. A. (2007) Variability in oceanic dissolved iron is dominated by the colloidal fraction. *Geochim. Cosmochim. Acta* **71**, 2960–2974.

Black E. E. (2018) *An investigation of basin-scale controls on upper ocean export and remineralization*. Massachusetts Institute of Technology.

Boyle E. A., Bergquist B. A., Kayser R. A. and Mahowald N. (2005) Iron, manganese, and lead at Hawaii Ocean Time-series station ALOHA: Temporal variability and an intermediate water hydrothermal plume. *Geochim. Cosmochim. Acta* **69**, 933–952.

Bruland K. W. and Lohan M. C. (2003) 6.02 – Controls of trace metals in seawater. In *Treatise on Geochemistry* (ed. H. D. H. K. Turekian). Pergamon, Oxford, pp. 23–47.

Bruland K. W., Orians K. J. and Cowen J. P. (1994) Reactive trace metals in the stratified central North Pacific. *Geochim. Cosmochim. Acta* **58**, 3171–3182.

Bucciarelli E., Blain S. and Tréguer P. (2001) Iron and manganese in the wake of the Kerguelen Islands (Southern Ocean). *Mar. Chem.* **73**, 21–36.

Burdige D. J. (2006) *Geochemistry of Marine Sediments*. Princeton University Press.

Byrne R. H. (2002) Inorganic speciation of dissolved elements in seawater: the influence of pH on concentration ratios. *Geochem. Trans.* **3**, 11.

Carpenter J. H. (1965) The Chesapeake Bay Institute technique for the Winkler dissolved oxygen method. *Limnol. Oceanogr.* **10**, 141–143.

Charette, M.A., Kipp, L.E., Jensen, L.T., Dabrowski, J.S., Whitmore, L.M., Fitzsimmons, J.N., Williford, T., Ulfsbo, A., Jones, E., Bundy, R.M., Vivancos, S.M., Pahnke, K., John,

S.G., Xiang, Y., Hatta, M., Petrova, M.V., Heimbürger-Boavida, L.-E., Bauch, D., Newton, R., Pasqualini, A., Agather, A.M., Amon, R.M.W., Anderson, R.F., Andersson, P.S., Benner, R., Bowman, K.L., Edwards, R.L., Gdaniec, S., Gerringa, L.J.A., González, A.G., Granskog, M., Haley, B., Hammerschmidt, C.R., Hansell, D.A., Henderson, P.B., Kadko, D.C., Kaiser, K., Laan, P., Lam, P.J., Lamborg, C. H., Levier, M., Li, X., Margolin, A.R., Measures, C., Middag, R., Millero, F.J., Moore, W.S., Paffrath, R., Planquette, H., Rabe, B., Reader, H., Rember, R., Rijkenberg, M.J.A., Roy-Barman, M., Rutgers van der Loeff, M., Saito, M., Schauer, U., Schlosser, P., Sherrell, R.M., Shiller, A.M., Slagter, H., Sonke, J.E., Stedmon, C., Woosley, R.J., Valk, O., van Ooijen, J. and Zhang, R. (2020) The transpolar drift as a source of riverine and shelf-derived trace elements to the Central Arctic Ocean. *J. Geophys. Res.: Oceans*, e2019JC015920.

Chase Z., Johnson K. S., Elrod V. A., Plant J. N., Fitzwater S. E., Pickell L. and Sakamoto C. M. (2005) Manganese and iron distributions off central California influenced by upwelling and shelf width. *Mar. Chem.* **95**, 235–254.

Cheize M., Planquette H. F., Fitzsimmons J. N., Pelleter E., Sherrell R. M., Lambert C., Bucciarelli E., Sarthou G., Le Goff M., Liorzou C., Chéron S., Viollier E. and Gayet N. (2019) Contribution of resuspended sedimentary particles to dissolved iron and manganese in the ocean: An experimental study. *Chem. Geol.* **511**, 389–415.

Chen L., Zhang J. and Zheng X. (2019) A laboratory study of the presence and transformation of dissolved Mn(III) across the sediment–water interface of an anoxic freshwater body. *Environ. Earth Sci.* **78**, 108.

Cid A. P., Nakatsuka S. and Sohrin Y. (2012) Stoichiometry among bioactive trace metals in the Chukchi and Beaufort Seas. *J. Oceanogr.* **68**, 985–1001.

Colombo M., Jackson S. L., Cullen J. T. and Orians K. J. (2020) Dissolved iron and manganese in the Canadian Arctic Ocean: On the biogeochemical processes controlling their distributions. *Geochim. Cosmochim. Acta* **277**, 150–174.

Corlett W. B. and Pickart R. S. (2017) The Chukchi slope current. *Prog. Oceanogr.* **153**, 50–65.

Cowen J. P. and Bruland K. W. (1985) Metal deposits associated with bacteria: implications for Fe and Mn marine biogeochemistry. *Deep Sea Res. Part A Oceanogr. Res. Pap.* **32**, 253–272.

Culberson, C.H., Knapp, G.P., Stalcup, M.C., Williams, R.T., Zemlyak, F., 1991. A comparison of methods for the determination of dissolved oxygen in seawater.

Cutter G., Andersson P., Codispoti L., Croot P., Francois R., Lohan M., Obata H. and Rutgers vd Loeff M. (2010) Sampling and sample-handling protocols for GEOTRACES cruises. *GEOTRACES*.

Fitzsimmons J. N. and Boyle E. A. (2012) An intercalibration between the GEOTRACES GO-FLO and the MITESS/Vanes sampling systems for dissolved iron concentration analyses (and a closer look at adsorption effects). *Limnol. Oceanogr. Methods* **10**, 437–450.

Fitzsimmons J. N. and Boyle E. A. (2014a) Assessment and comparison of Anopore and cross flow filtration methods for the determination of dissolved iron size fractionation into soluble and colloidal phases in seawater. *Limnol. Oceanogr. Methods* **12**, 246–263.

Fitzsimmons J. N. and Boyle E. A. (2014b) Both soluble and colloidal iron phases control dissolved iron variability in the tropical North Atlantic Ocean. *Geochim. Cosmochim. Acta* **125**, 539–550.

Fitzsimmons J. N., Boyle E. A. and Jenkins W. J. (2014) Distal transport of dissolved hydrothermal iron in the deep South Pacific Ocean. *Proc. Natl. Acad. Sci.* **111**, 16654–16661.

Fitzsimmons J. N., Carrasco G. G., Wu J., Roshan S., Hatta M., Measures C. I., Conway T. M., John S. G. and Boyle E. A. (2015) Partitioning of dissolved iron and iron isotopes into soluble and colloidal phases along the GA03 GEOTRACES North Atlantic Transect. *Deep-Sea Res. Part II: Top. Stud. Oceanogr.* **116**, 130–151.

Fitzsimmons J. N., John S. G., Marsay C. M., Hoffman C. L., Nicholas S. L., Toner B. M., German C. R. and Sherrell R. M. (2017) Iron persistence in a distal hydrothermal plume supported by dissolved–particulate exchange. *Nat. Geosci.* **10**, 195.

Froelich P. N., Klinkhammer G., Bender M. L., Luedtke N., Heath G. R., Cullen D., Dauphin P., Hammond D., Hartman B. and Maynard V. (1979) Early oxidation of organic matter in pelagic sediments of the eastern equatorial Atlantic: suboxic diagenesis. *Geochim. Cosmochim. Acta* **43**, 1075–1090.

German C. R., Casciotti K. A., Dutay J.-C., Heimbürger L. E., Jenkins W. J., Measures C. I., Mills R. A., Obata H., Schlitzer R., Tagliabue A., Turner D. R. and Whitby H. (2016) Hydrothermal impacts on trace element and isotope ocean biogeochemistry. *Philos. Trans. R. Soc. A: Math. Phys. Eng. Sci.* **374**, 20160035.

Gledhill M. and Buck K. N. (2012) The organic complexation of iron in the marine environment: a review. *Front. Microbiol.* **3**, 69.

Goldberg E. D. (1954) Marine geochemistry 1. Chemical Scavengers of the Sea. *J. Geol.* **62**, 249–265.

Gordon R., Johnson K. and Coale K. (1998) The behaviour of iron and other trace elements during the IronEx-I and PlumEx experiments in the Equatorial Pacific. *Deep Sea Research Part II: Topical Studies in Oceanography* **45**(6), 995–1041.

Granger J., Sigman D. M., Gagnon J., Tremblay J.-E. and Mucci A. (2018) On the properties of the arctic halocline and deep water masses of the Canada Basin from Nitrate Isotope Ratios. *J. Geophys. Res. Oceans* **123**, 5443–5458.

Harrison W. and Cota G. (1991) Primary production in polar waters: relation to nutrient availability. *Polar Res.* **10**, 87–104.

Hatta M., Measures C., Selph K., Zhou M. and Hiscock W. (2013) Iron fluxes from the shelf regions near the South Shetland Islands in the Drake Passage during the austral-winter 2006. *Deep Sea Res. Part II* **90**, 89–101.

Hatta M., Measures C. I., Wu J., Roshan S., Fitzsimmons J. N., Sedwick P. and Morton P. (2015) An overview of dissolved Fe and Mn distributions during the 2010–2011 US GEOTRACES north Atlantic cruises: GEOTRACES GA03. *Deep Sea Res. Part II* **116**, 117–129.

Hein J. R., Konstantinova N., Mikesell M., Mizell K., Fitzsimmons J. N., Lam P. J., Jensen L. T., Xiang Y., Gartman A., Cherkashov G., Hutchinson D. R. and Till C. P. (2017) Arctic deep water ferromanganese-oxide deposits reflect the unique characteristics of the Arctic Ocean. *Geochem. Geophys. Geosyst.* **18**, 3771–3800.

Hill V. and Cota G. (2005) Spatial patterns of primary production on the shelf, slope and basin of the Western Arctic in 2002. *Deep Sea Res. Part II* **52**, 3344–3354.

Hioki N., Kuma K., Morita Y., Sasayama R., Ooki A., Kondo Y., Obata H., Nishioka J., Yamashita Y., Nishino S., Kikuchi T. and Aoyama M. (2014) Laterally spreading iron, humic-like dissolved organic matter and nutrients in cold, dense subsurface water of the Arctic Ocean. *Sci. Rep.* **4**, 6775.

Hydes, D., Aoyama, M., Aminot, A., Bakker, K., Becker, S., Coverly, S., Daniel, A., Dickson, A., Grosso, O. and Kerouel, R. (2010) Determination of dissolved nutrients (N, P, Si) in seawater with high precision and inter-comparability using gas-segmented continuous flow analysers.

Jakobsson M., Grantz A., Kristoffersen Y., Macnab R., MacDonald R., Sakshaug E., Stein R. and Jokat W. (2004) *The Arctic*

Ocean: Boundary Conditions and Background Information,The Organic Carbon Cycle in the Arctic Ocean. Springer, pp. 1–32.

Jensen L. T., Wyatt N. J., Landing W. M. and Fitzsimmons J. N. (2020) Assessment of the stability, sorption, and exchangeability of marine dissolved and colloidal metals. *Mar. Chem.* **220**, 103754.

Jensen L. T., Wyatt N. J., Twining B. S., Rauschenberg S., Landing W. M., Sherrell R. M. and Fitzsimmons J. N. (2019) Biogeochemical Cycling of Dissolved Zinc in the Western Arctic (Arctic GEOTRACES GN01). *Global Biogeochem. Cycles* **33**, 343–369.

Johnson K. S., Gordon R. M. and Coale K. H. (1997) What controls dissolved iron concentrations in the world ocean? *Mar. Chem.* **57**, 137–161.

Jones E. P. and Anderson L. G. (1986) On the origin of the chemical properties of the Arctic Ocean halocline. *J. Geophys. Res. Oceans* **91**, 10759–10767.

Kadko, D., Millero, F.J., Woosley, R., Hansell, D.A., Swift, J.H., Landing, W.M., Smethie, W.M.J., Schlosser, P., 2016. Dissolved inorganic carbon, pH, alkalinity, temperature, salinity and other variables collected from discrete sample and profile observations using CTD, bottle and other instruments from HEALY in the Arctic Ocean, Beaufort Sea and Bering Sea from 2015-08-09 to 2015-10-13. In: Information, NOAA National Centers for Environmental Information, Version 2.2. doi: 10.3334/CDIAC/OTG.CLIVAR_ARC01_33HQ20150809.

Kanna N., Toyota T. and Nishioka J. (2014) Iron and macronutrient concentrations in sea ice and their impact on the nutritional status of surface waters in the southern Okhotsk Sea. *Prog. Oceanogr.* **126**, 44–57.

Klunder M. B., Bauch D., Laan P., de Baar H. J. W., van Heuven S. and Ober S. (2012a) Dissolved iron in the Arctic shelf seas and surface waters of the central Arctic Ocean: Impact of Arctic river water and ice-melt. *J. Geophys. Res. Oceans* **117**.

Klunder M. B., Laan P., Middag R., de Baar H. J. W. and Bakker K. (2012b) Dissolved iron in the Arctic Ocean: Important role of hydrothermal sources, shelf input and scavenging removal. *J. Geophys. Res. Oceans* **117**.

Kondo Y., Obata H., Hioki N., Ooki A., Nishino S., Kikuchi T. and Kuma K. (2016) Transport of trace metals (Mn, Fe, Ni, Zn and Cd) in the western Arctic Ocean (Chukchi Sea and Canada Basin) in late summer 2012. *Deep Sea Res. Part I* **116**, 236–252.

Koschinsky A. and Hein J. R. (2003) Uptake of elements from seawater by ferromanganese crusts: solid-phase associations and seawater speciation. *Mar. Geol.* **198**, 331–351.

Kuma K., Nishioka J. and Matsunaga K. (1996) Controls on iron (III) hydroxide solubility in seawater: the influence of pH and natural organic chelators. *Limnol. Oceanogr.* **41**, 396–407.

Lagerström M., Field M., Seguret M., Fisher L., Hann S. and Sherrell R. M. (2013) Automated on-line flow-injection ICP-MS determination of trace metals (Mn, Fe Co, Ni, Cu and Zn) in open ocean seawater: Application to the GEOTRACES program. *Mar. Chem.* **155**, 71–80.

Lam P. J. and Bishop J. K. B. (2008) The continental margin is a key source of iron to the HNLC North Pacific Ocean. *Geophys. Res. Lett.* **35**.

Landing W. M. and Bruland K. W. (1987) The contrasting biogeochemistry of iron and manganese in the Pacific Ocean. *Geochim. Cosmochim. Acta* **51**, 29–43.

Lannuzel D., Bowie A. R., van der Merwe P. C., Townsend A. T. and Schoemann V. (2011) Distribution of dissolved and particulate metals in Antarctic sea ice. *Mar. Chem.* **124**, 134–146.

Lepore K., Moran S., Grebmeier J., Cooper L., Lalande C., Maslowski W., Hill V., Bates N., Hansell D. A. and Mathis J. (2007) Seasonal and interannual changes in particulate organic carbon export and deposition in the Chukchi Sea. *J. Geophys. Res. Oceans* **112**.

Lewis B. L. and Landing W. M. (1991) The biogeochemistry of manganese and iron in the Black Sea. *Deep Sea Res. Part A Oceanogr. Res. Pap.* **38**, S773–S803.

Liu X. and Millero F. J. (2002) The solubility of iron in seawater. *Mar. Chem.* **77**, 43–54.

Luther G. W., Madison A. S., Mucci A., Sundby B. and Oldham V. E. (2015) A kinetic approach to assess the strengths of ligands bound to soluble Mn(III). *Mar. Chem.* **173**, 93–99.

Macdonald R. W., Carmack E. C., McLaughlin F. A., Iseki K., Macdonald D. M. and O'Brien M. C. (1989) Composition and modification of water masses in the Mackenzie shelf estuary. *J. Geophys. Res. Oceans* **94**, 18057–18070.

Macdonald R. W. and Gobeil C. (2012) Manganese Sources and Sinks in the Arctic Ocean with Reference to Periodic Enrichments in Basin Sediments. *Aquat. Geochem.* **18**, 565–591.

Madison A. S., Tebo B. M., Mucci A., Sundby B. and Luther G. W. (2013) Abundant porewater Mn(III) is a major component of the sedimentary redox system. *Science* **341**, 875–878.

Magen C., Mucci A. and Sundby B. (2011) Reduction rates of sedimentary Mn and Fe oxides: An incubation experiment with Arctic Ocean Sediments. *Aquat. Geochem.* **17**, 629–643.

Marsay C. M., Aguilar-Islas A., Fitzsimmons J. N., Hatta M., Jensen L. T., John S. G., Kadko D., Landing W. M., Lanning N. T., Morton P. L., Pasqualini A., Rauschenberg S., Sherrell R. M., Shiller A. M., Twining B. S., Whitmore L. M., Zhang R. and Buck C. S. (2018) Dissolved and particulate trace elements in late summer Arctic melt ponds. *Mar. Chem.* **204**, 70–85.

Martin J. H. and Knauer G. A. (1985) Lateral transport of Mn in the north-east Pacific Gyre oxygen minimum. *Nature* **314**, 524–526.

Measures C. (1999) The role of entrained sediments in sea ice in the distribution of aluminium and iron in the surface waters of the Arctic Ocean. *Mar. Chem.* **68**, 59–70.

Middag R., de Baar H. J. W., Laan P. and Klunder M. B. (2011) Fluvial and hydrothermal input of manganese into the Arctic Ocean. *Geochim. Cosmochim. Acta* **75**, 2393–2408.

Millero F. J., Sotolongo S. and Izaguirre M. (1987) The oxidation kinetics of Fe(II) in seawater. *Geochim. Cosmochim. Acta* **51**, 793–801.

Münchow A. and Carmack E. C. (1997) Synoptic flow and density observations near an Arctic shelf break. *J. Phys. Oceanogr.* **27**, 1402–1419.

Nakawo M. and Sinha N. K. (1981) Growth rate and salinity profile of first-year Sea ice in the high Arctic. *J. Glaciol.* **27**, 315–330.

Nakayama Y., Fujita S., Kuma K. and Shimada K. (2011) Iron and humic-type fluorescent dissolved organic matter in the Chukchi Sea and Canada Basin of the western Arctic Ocean. *J. Geophys. Res. Oceans* **116**.

Nealson K. H., Tebo B. M. and Rosson R. A. (1988) Occurrence and Mechanisms of Microbial Oxidation of Manganese. In *Advances in Applied Microbiology* (ed. A. I. Laskin). Academic Press, pp. 279–318.

Newton R., Schlosser P., Mortlock R., Swift J. and MacDonald R. (2013) Canadian Basin freshwater sources and changes: Results from the 2005 Arctic Ocean Section. *J. Geophys. Res. Oceans* **118**, 2133–2154.

Nishimura S., Kuma K., Ishikawa S., Omata A. and Saitoh S.-I. (2012) Iron, nutrients, and humic-type fluorescent dissolved organic matter in the northern Bering Sea shelf, Bering Strait, and Chukchi Sea. *J. Geophys. Res. Oceans* **117**.

Nishino S., Shimada K. and Itoh M. (2005) Use of ammonium and other nitrogen tracers to investigate the spreading of shelf waters in the western Arctic halocline. *J. Geophys. Res. Oceans* **110**.

Noble A. E., Lamborg C. H., Ohnemus D. C., Lam P. J., Goepfert T. J., Measures C. I., Frame C. H., Casciotti K. L., DiTullio G. R., Jennings J. and Saito M. A. (2012) Basin-scale inputs of cobalt, iron, and manganese from the Benguela-Angola front to the South Atlantic Ocean. *Limnol. Oceanogr.* **57**, 989–1010.

Noble A. E., Saito M. A., Maiti K. and Benitez-Nelson C. R. (2008) Cobalt, manganese, and iron near the Hawaiian Islands: A potential concentrating mechanism for cobalt within a cyclonic eddy and implications for the hybrid-type trace metals. *Deep Sea Res. Part II* **55**, 1473–1490.

Ohnemus D. C. and Lam P. J. (2015) Cycling of lithogenic marine particles in the US GEOTRACES North Atlantic transect. *Deep Sea Res. Part II* **116**, 283–302.

Oldham V. E., Mucci A., Tebo B. M. and Luther Iii G. W. (2017) Soluble Mn(III)–L complexes are abundant in oxygenated waters and stabilized by humic ligands. *Geochim. Cosmochim. Acta* **199**, 238–246.

Oldham V. E., Owings S. M., Jones M. R., Tebo B. M. and Luther G. W., III (2015) Evidence for the presence of strong Mn (III)-binding ligands in the water column of the Chesapeake Bay. *Mar. Chem.* **171**, 58–66.

Planquette H. and Sherrell R. M. (2012) Sampling for particulate trace element determination using water sampling bottles: methodology and comparison to in situ pumps. *Limnol. Oceanogr. Methods* **10**, 367–388.

Raiswell R. (2011) Iron transport from the continents to the open ocean: The aging–rejuvenation cycle. *Elements* **7**, 101–106.

Rijkenberg M. J. A., Slagter H. A., Rutgers van der Loeff M., van Ooijen J. and Gerringa L. J. A. (2018) Dissolved Fe in the deep and upper Arctic Ocean with a focus on Fe limitation in the Nansen Basin. *Front. Mar. Sci.* **5**.

Rudels B. (2015) Arctic Ocean circulation, processes and water masses: A description of observations and ideas with focus on the period prior to the International Polar Year 2007–2009. *Prog. Oceanogr.* **132**, 22–67.

Rudnick R. and Gao S. (2003) Composition of the continental crust. *The Crust* **3**, 1–64.

Rue E. L. and Bruland K. W. (1995) Complexation of iron (III) by natural organic ligands in the Central North Pacific as determined by a new competitive ligand equilibration/adsorptive cathodic stripping voltammetric method. *Mar. Chem.* **50**, 117–138.

Saager P. M., De Baar H. J. W. and Burkill P. H. (1989) Manganese and iron in Indian Ocean waters. *Geochim. Cosmochim. Acta* **53**, 2259–2267.

Sakshaug E. (2004) *Primary and Secondary Production in the Arctic Seas, The Organic Carbon Cycle in the Arctic Ocean*. Springer, pp. 57–81.

Sanial V., Kipp L., Henderson P., van Beek P., Reyss J.-L., Hammond D., Hawco N., Saito M., Resing J. and Sedwick P. (2017) Radium-228 as a tracer of dissolved trace element inputs from the Peruvian continental margin. *Mar. Chem.*.

Schlitzer, R., 2016. Ocean data view. http://odv.awi.de.

Scholz F., Hensen C., Noffke A., Rohde A., Liebetrau V. and Wallmann K. (2011) Early diagenesis of redox-sensitive trace metals in the Peru upwelling area – response to ENSO-related oxygen fluctuations in the water column. *Geochim. Cosmochim. Acta* **75**, 7257–7276.

Sedwick P. N., DiTullio G. R. and Mackey D. J. (2000) Iron and manganese in the Ross Sea, Antarctica: seasonal iron limitation in Antarctic shelf waters. *J. Geophys. Res. Oceans* **105**, 11321–11336.

Sedwick P. N., Edwards P. R., Mackey D. J., Griffiths F. B. and Parslow J. S. (1997) Iron and manganese in surface waters of the Australian subantarctic region. *Deep Sea Res. Part I* **44**, 1239–1253.

Sherrell R. M., Annett A. L., Fitzsimmons J. N., Roccanova V. J. and Meredith M. P. (2018) A "shallow bathtub ring" of local sedimentary iron input maintains the Palmer Deep biological hotspot on the West Antarctic Peninsula shelf. *Philos. Trans. R. Soc. A: Math. Phys. Eng. Sci.* **376**, 20170171.

Shiller A. M. (1997) Manganese in surface waters of the Atlantic Ocean. *Geophys. Res. Lett.* **24**, 1495–1498.

Shimada K., Itoh M., Nishino S., McLaughlin F., Carmack E. and Proshutinsky A. (2005) Halocline structure in the Canada Basin of the Arctic Ocean. *Geophys. Res. Lett.* **32**.

Sholkovitz E., Boyle E. and Price N. (1978) The removal of dissolved humic acids and iron during estuarine mixing. *Earth Planet. Sci. Lett.* **40**, 130–136.

Sholkovitz E. R. (1978) The flocculation of dissolved Fe, Mn, Al, Cu, NI, Co and Cd during estuarine mixing. *Earth Planet. Sci. Lett.* **41**, 77–86.

Slagter H. A., Laglera L. M., Sukekava C. and Gerringa L. J. A. (2019) Fe-binding organic ligands in the humic-rich transpolar drift in the surface Arctic Ocean using multiple voltammetric methods. *J. Geophys. Res. Oceans* **124**, 1491–1508.

Slagter H. A., Reader H. E., Rijkenberg M. J. A., Rutgers van der Loeff M., de Baar H. J. W. and Gerringa L. J. A. (2017) Organic Fe speciation in the Eurasian Basins of the Arctic Ocean and its relation to terrestrial DOM. *Mar. Chem.* **197**, 11–25.

Stumm, W., Morgan, J., 1981. Aquatic Chemistry, 780, J. Wiley & Sons.

Sunda W., Huntsman S. and Harvey G. (1983) Photoreduction of manganese oxides in seawater and its geochemical and biological implications. *Nature* **301**, 234–236.

Sunda W. G. (2012) Feedback interactions between trace metal nutrients and phytoplankton in the ocean. *Front. Microbiol.* **3**.

Sunda W. G. and Huntsman S. A. (1994) Photoreduction of manganese oxides in seawater. *Mar. Chem.* **46**, 133–152.

Sunda W. G. and Huntsman S. A. (1995) Iron uptake and growth limitation in oceanic and coastal phytoplankton. *Mar. Chem.* **50**, 189–206.

Sunda W. G. and Huntsman S. A. (1998) Interactions among Cu2+, Zn2+, and Mn2+ in controlling cellular Mn, Zn, and growth rate in the coastal alga Chlamydomonas. *Limnol. Oceanogr.* **43**, 1055–1064.

Tagliabue A., Bowie A. R., Boyd P. W., Buck K. N., Johnson K. S. and Saito M. A. (2017) The integral role of iron in ocean biogeochemistry. *Nature* **543**, 51–59.

Talley L. D., Pickard G. L., Emery W. J. and Swift J. H. (2011) *Chapter 12 - Arctic Ocean and Nordic Seas, Descriptive Physical Oceanography (Sixth Edition)*. Academic Press, Boston, pp. 401–436.

Tebo B. M. (1991) Manganese(II) oxidation in the suboxic zone of the Black Sea. *Deep Sea Res. Part A Oceanogr. Res. Pap.* **38**, S883–S905.

Tebo B. M., Bargar J. R., Clement B. G., Dick G. J., Murray K. J., Parker D., Verity R. and Webb S. M. (2004) BIOGENIC MANGANESE OXIDES: Properties and mechanisms of formation. *Annu. Rev. Earth Planet. Sci.* **32**, 287–328.

Tovar-Sánchez A., Duarte C. M., Alonso J. C., Lacorte S., Tauler R. and Galbán-Malagón C. (2010) Impacts of metals and nutrients released from melting multiyear Arctic sea ice. *J. Geophys. Res. Oceans* **115**.

Trefry J. H., Trocine R. P., Cooper L. W. and Dunton K. H. (2014) Trace metals and organic carbon in sediments of the northeastern Chukchi Sea. *Deep Sea Res. Part II* **102**, 18–31.

Twining B. S., Rauschenberg S. and Morton P. (2017) *Trace Metal Contents of Biogenic Particles and Phytoplankton in the Upper Arctic Ocean and Arctic Sea Ice*. ASLO Aquatic Sciences, Honolulu, HI.

Twining B. S., Rauschenberg S., Morton P. L. and Vogt S. (2015) Metal contents of phytoplankton and labile particulate material in the North Atlantic Ocean. *Prog. Oceanogr.* **137**, 261–283.

Vancoppenolle M., Fichefet T. and Bitz C. M. (2006) Modeling the salinity profile of undeformed Arctic sea ice. *Geophys. Res. Lett.* **33**.

Vandieken V., Nickel M. and Jørgensen B. B. (2006) Carbon mineralization in Arctic sediments northeast of Svalbard: Mn (IV) and Fe (III) reduction as principal anaerobic respiratory pathways. *Mar. Ecol. Prog. Ser.* **322**, 15–27.

Vieira L. H., Achterberg E. P., Scholten J., Beck A. J., Liebetrau V., Mills M. M. and Arrigo K. R. (2019) Benthic fluxes of trace metals in the Chukchi Sea and their transport into the Arctic Ocean. *Mar. Chem.* **208**, 43–55.

von Langen P. J., Johnson K. S., Coale K. H. and Elrod V. A. (1997) Oxidation kinetics of manganese (II) in seawater at nanomolar concentrations. *Geochim. Cosmochim. Acta* **61**, 4945–4954.

Wells M. L. (2002) Marine colloids and trace metals. *Biogeochem. Mar. Dissolved Org. Matter*, 367–404.

Whitmore L. M., Morton P. L., Twining B. S. and Shiller A. M. (2019) Vanadium cycling in the Western Arctic Ocean is influenced by shelf-basin connectivity. *Mar. Chem.* **216**, 103701.

Woodgate R. A., Aagaard K., Swift J. H., Falkner K. K. and Smethie W. M. (2005) Pacific ventilation of the Arctic Ocean's lower halocline by upwelling and diapycnal mixing over the continental margin. *Geophys. Res. Lett.* **32**.

Wu J. and Luther, III, G. W. (1996) Spatial and temporal distribution of iron in the surface water of the northwestern Atlantic Ocean. *Geochimica et Cosmochimica Acta* **60**(15), 2729–2741.

Xiang Y. and Lam P. J. (2020) Size-fractionated compositions of marine suspended particles in the Western Arctic Ocean: lateral and vertical sources. *J. Geophys Res. Oceans*, e2020JC016144.

Yamashita Y., Nishioka J., Obata H. and Ogawa H. (2020) Shelf humic substances as carriers for basin-scale iron transport in the North Pacific. *Sci. Rep.* **10**, 4505.

Yeats P. and Strain P. (1990) The oxidation of manganese in seawater: rate constants based on field data. *Estuar. Coast. Shelf Sci.* **31**, 11–24.

Yu H. and Leadbetter J. R. (2020) Bacterial chemolithoautotrophy via manganese oxidation. *Nature* **583**, 453–458.

Zhang R., Jensen L. T., Fitzsimmons J. N., Sherrell R. M. and John S. (2019) Dissolved cadmium and cadmium stable isotopes in the western Arctic Ocean. *Geochim. Cosmochim. Acta* **258**, 258–273.

Associate editor: Jeffrey G. Catalano